



ELSEVIER

journal homepage: [www.intl.elsevierhealth.com/journals/cmpb](http://www.intl.elsevierhealth.com/journals/cmpb)

# Blood vessel segmentation methodologies in retinal images – A survey

M.M. Fraz<sup>a,\*</sup>, P. Remagnino<sup>a</sup>, A. Hoppe<sup>a</sup>, B. Uyyanonvara<sup>b</sup>, A.R. Rudnicka<sup>c</sup>,  
C.G. Owen<sup>c</sup>, S.A. Barman<sup>a</sup>

<sup>a</sup> Digital Imaging Research Centre, Faculty of Science, Engineering and Computing, Kingston University London, London, United Kingdom

<sup>b</sup> Department of Information Technology, Sirindhorn International Institute of Technology, Thammasat University, Bangkok, Thailand

<sup>c</sup> Division of Population Health Sciences and Education, St. George's, University of London, London, United Kingdom

## ARTICLE INFO

### Article history:

Received 5 October 2011

Received in revised form

5 March 2012

Accepted 24 March 2012

### Keywords:

Medical imaging

Retinal images

Image segmentation

Blood vessel segmentation

Retinopathy

Survey

## ABSTRACT

Retinal vessel segmentation algorithms are a fundamental component of automatic retinal disease screening systems. This work examines the blood vessel segmentation methodologies in two dimensional retinal images acquired from a fundus camera and a survey of techniques is presented. The aim of this paper is to review, analyze and categorize the retinal vessel extraction algorithms, techniques and methodologies, giving a brief description, highlighting the key points and the performance measures. We intend to give the reader a framework for the existing research; to introduce the range of retinal vessel segmentation algorithms; to discuss the current trends and future directions and summarize the open problems. The performance of algorithms is compared and analyzed on two publicly available databases (DRIVE and STARE) of retinal images using a number of measures which include accuracy, true positive rate, false positive rate, sensitivity, specificity and area under receiver operating characteristic (ROC) curve.

© 2012 Elsevier Ireland Ltd. All rights reserved.

## 1. Introduction

Retinal vessel segmentation and delineation of morphological attributes of retinal blood vessels, such as length, width, tortuosity and/or branching pattern and angles are utilized for diagnosis, screening, treatment, and evaluation of various cardiovascular and ophthalmologic diseases such as diabetes, hypertension, arteriosclerosis and choroidal neovascularization [1]. Automatic detection and analysis of the vasculature can assist in the implementation of screening programs for diabetic retinopathy [2], evaluation of retinopathy of prematurity [3], foveal avascular region detection [4], arteriolar narrowing [5], the relationship between vessel tortuosity and hypertensive retinopathy [6], vessel diameter measurement

in relation with diagnosis of hypertension [7], and computer-assisted laser surgery [1]. Automatic generation of retinal maps and extraction of branch points have been used for temporal or multimodal image registration [8], retinal image mosaic synthesis [9], optic disk identification and fovea localization [10]. Moreover, the retinal vascular tree is found to be unique for each individual and can be used for biometric identification [11,12].

Manual segmentation of retinal blood vessels is a long and tedious task which also requires training and skill. It is commonly accepted by the medical community that automatic quantification of retinal vessels is the first step in the development of a computer-assisted diagnostic system for ophthalmic disorders. A large number of algorithms and techniques have been published

\* Corresponding author. Tel.: +44 7514567523.

E-mail address: [moazam.fraz@kingston.ac.uk](mailto:moazam.fraz@kingston.ac.uk) (M.M. Fraz).

0169-2607/\$ – see front matter © 2012 Elsevier Ireland Ltd. All rights reserved.

<http://dx.doi.org/10.1016/j.cmpb.2012.03.009>

relating to the segmentation of retinal blood vessels. In this paper, we have presented a survey of algorithms particularly focusing on the extraction of blood vessels from two dimensional, colored, non-dilated retinal images acquired either from a fundus camera or using fluorescein angiography.

Reviews and surveys on the algorithms for segmentation of vessel like structures in medical images are present in the literature [13,14]. For instance, Kirbas and Quek [15] presented a comprehensive survey of the techniques and algorithms for extraction of vessels and elongated structures in 2-D as well as 3-D medical images focused in a variety of application domains. A brief survey on retinal segmentation and registration algorithms is presented by Mabrouk et al. [16] which limits discussion to the extraction of cores and edges of retinal blood vessels. The most recent studies [17,18] discuss the algorithms for automatic detection of diabetic retinopathy in retinal images. This survey is unique in that it particularly focuses on the algorithms and methodologies for the segmentation of blood vessels in two dimensional colored retinal images acquired from a fundus camera and no such review exists to the best of our knowledge. The objectives of this paper are to review the retinal vessel segmentation methodologies; to provide a detailed resource of the algorithms employed for vessel segmentation to researchers for ready reference; to discuss the advantages and disadvantages of the various approaches; to discuss the current trends and future directions and summarize the open problems.

The paper is structured in five sections; Section 2 describes the challenges associated with retinal vessel segmentation, the materials used for analysis, and quantitative measures of performance for vessel segmentation. The classification of the extraction methods and brief description of papers of each category is given in Section 3. The discussion is given in Section 4. Finally the conclusion and future directions are illustrated in Section 5.

---

## 2. Retinal image processing

### 2.1. Retinal photography

Retinal photography requires the use of a complex optical system, called a fundus camera. It is a specialized low power microscope with an attached camera, capable of simultaneously illuminating and imaging the retina. It is designed to image the interior surface of the eye, which includes the retina, optic disc, macula, and posterior pole [19]. The fundus camera normally operates in three modes. In Color photography the retina is examined in full color under the illumination of white light. In Red-free photography, the vessels and other structures are improved in contrast and the imaging light is filtered to remove the red colors. The fluorescent angiograms are acquired using the dye tracing method. A sodium fluorescein or indocyanine green is injected into the blood, and then the angiogram is obtained by photographing the fluorescence emitted after illumination of the retina with blue light at a wavelength of 490 nanometers.

### 2.2. Retinal vessel segmentation

The retinal vasculature is composed of arteries and veins appearing as elongated features, with their tributaries visible within the retinal image. There is a wide range of vessel widths ranging from one pixel to twenty pixels, depending on both the width of the vessel and the image resolution. Other structures appearing in ocular fundus images include the retina boundary, the optic disc, and pathologies in the form of cotton wool spots, bright and dark lesions and exudates as shown in Fig. 1(b–d). The vessel cross-sectional intensity profiles approximate a Gaussian shape or a mixture of Gaussians in the case where a central vessel reflex is present. The orientation and grey level of a vessel does not change abruptly; they are locally linear and gradually change in intensity along their lengths. The vessels can be expected to be connected and, in the retina, form a binary treelike structure. However, the shape, size and local grey level of blood vessels can vary hugely and some background features may have similar attributes to vessels as illustrated in Fig. 1(a and d).

Vessel crossing and branching can further complicate the profile model. As with the processing of most medical images, signal noise, drift in image intensity and lack of image contrast pose significant challenges to the extraction of blood vessels. Retinal vessels also show an evidence of a strong reflection along their centerline known as a central vessel reflex as evident in Fig. 1(a), which is more apparent in arteries than veins, is stronger at images taken at longer wavelengths, and typically found in the retinal images of younger patients.

### 2.3. Publicly available retinal image databases

A summary of all the publicly available retinal image databases known to us is given in this section. Most of the retinal vessel segmentation methodologies are evaluated on two databases (DRIVE and STARE).

#### 2.3.1. DRIVE database

The DRIVE (Digital Retinal Images for Vessel Extraction) [20] is a publicly available database, consisting of a total of 40 color fundus photographs. The photographs were obtained from a diabetic retinopathy screening program in the Netherlands. The screening population consisted of 453 subjects between 31 and 86 years of age. Each image has been JPEG compressed, which is common practice in screening programs. Of the 40 images in the database, 7 contain pathology, namely exudates, hemorrhages and pigment epithelium changes. See Fig. 2 for an example of both a normal and a pathological image. The images were acquired using a Canon CR5 non-mydratric 3-CCD camera with a 45° field of view (FOV). Each image is captured using 8 bits per color plane at 768 × 584 pixels. The FOV of each image is circular with a diameter of approximately 540 pixels. The set of 40 images was divided into a test and training set both containing 20 images. Three observers, the first and second author and a computer science student manually segmented a number of images. All observers were trained by an experienced ophthalmologist (the last author). The first observer segmented 14 images of the training set while the second observer segmented the other 6 images. The test set was segmented twice resulting in a set X and Y. Set X

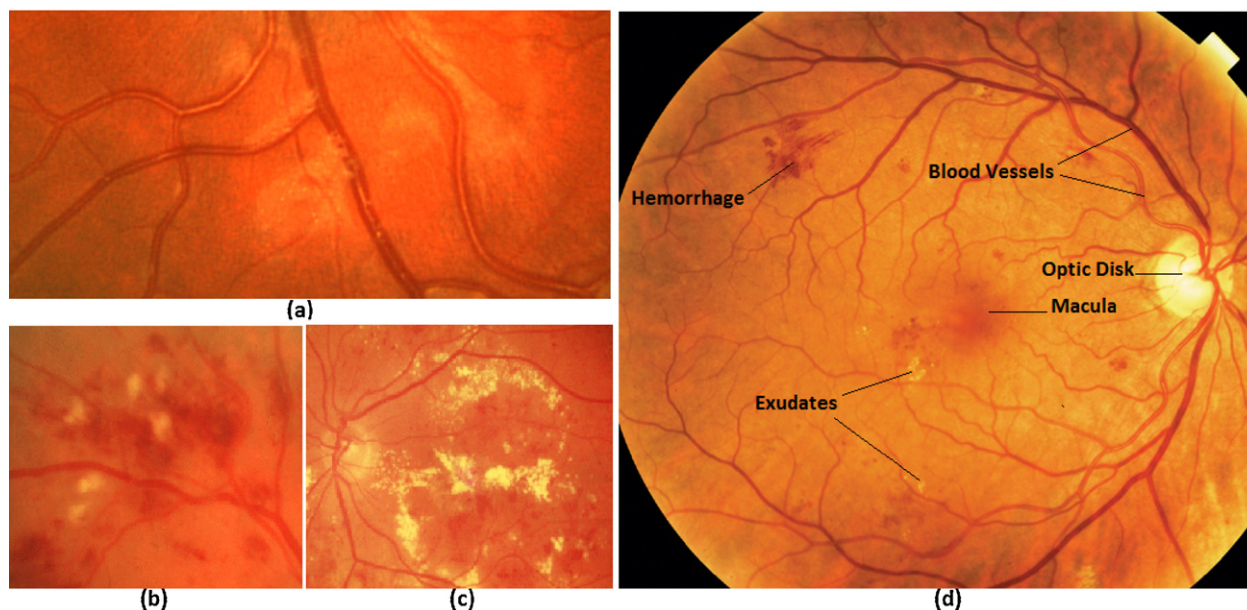


**Fig. 1 – Morphology of retinal images: (a) central vessel reflex and uneven background, (b) cotton wool spots, (c) hard exudates, (d) anatomical structures in the retina.**

was segmented by both the first and second observer (13 and 7 images, respectively) while set Y was completely segmented by the third observer. The performance of the vessel segmentation algorithms is measured on the test set. In set X the observers marked 577,649 pixels as vessel and 3,960,494 as background (12.7% vessel). In set Y 556,532 pixels are marked as vessel and 3,981,611 as background (12.3% vessel).

### 2.3.2. STARE database

The STARE database [21] contains 20 images for blood vessel segmentation; ten of these contain pathology. Fig. 3 shows retinal images from the STARE database. The digitized slides are captured by a TopCon TRV-50 fundus camera at 35° field of view. The slides were digitized to 605 × 700 pixels, 8 bits per color channel. The approximate diameter of the FOV is 650 × 500 pixels. Two observers manually segmented all the images. The first observer segmented 10.4% of pixels as vessel,

against 14.9% vessels for the second observer. The difference in segmentation between the two observers is due to the fact that the second observer segmented many more of the thinner vessels than the first one. Performance is computed with the segmentation of the first observer as the ground truth.

### 2.3.3. ARIA online

This database was created in 2006, in a research collaboration between St. Paul's Eye Unit, Royal Liverpool University Hospital Trust, Liverpool, UK and the Department of Ophthalmology, Clinical Sciences, University of Liverpool, Liverpool, UK [22]. The database consists of three groups; one has 92 images with age-related macular degeneration, the second group has 59 images with diabetes and a control group consists of 61 images. The trace of blood vessels, the optic disc and fovea location is marked by two image analysis experts as the reference standard. The images are captured

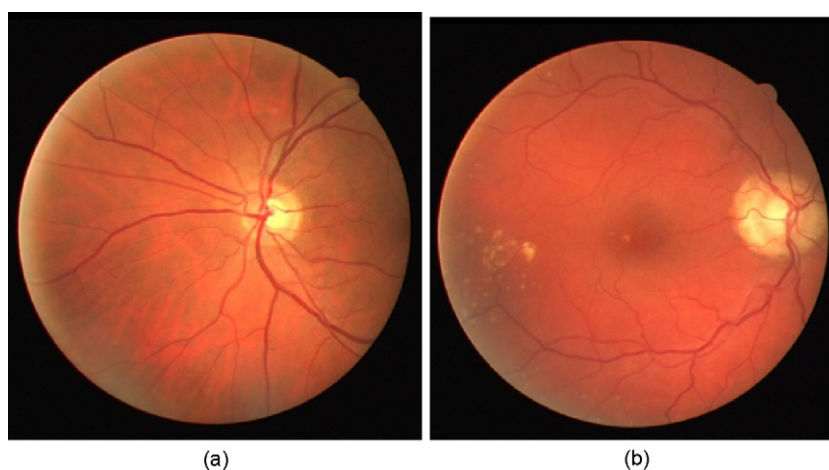


**Fig. 2 – Retinal images from DRIVE: (a) healthy retina, (b) retina showing pathologies.**

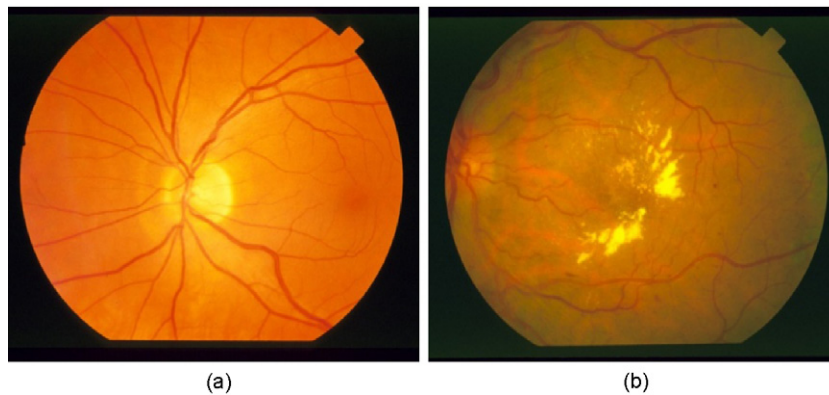


**Fig. 3 – Retinal Images from STARE: (a) healthy retina, (b) pathological retina.**

at a resolution of  $768 \times 576$  pixels in RGB color with 8-bits per color plane with a Zeiss FF450+ fundus camera at a  $50^\circ$  FOV and stored as uncompressed TIFF files.

#### 2.3.4. ImageRet

The ImageRet database was made publicly available in 2008 and is subdivided into two sub-databases, DIARETDB0 and DIARETDB1 [23]. DIARETDB0 contains 130 retinal images of which 20 are normal and 110 contain various symptoms of diabetic retinopathy. DIARETDB1 contains 89 images out of which 5 images are of a healthy retina while the other 84 have at least some signs of mild proliferative diabetic retinopathy. The images are marked by four experts for the presence of microaneurysms, hemorrhages, and hard and soft exudates. The images are acquired with a  $50^\circ$  FOV using a fundus camera with unknown settings at a size of  $1500 \times 1152$  pixels in PNG format.

#### 2.3.5. Messidor

The Messidor-project database [24] is the largest database of 1200 retinal images currently available on the internet and is provided courtesy of the Messidor program partners. The images were acquired at three different ophthalmology departments using a non-mydratic 3CCD camera (Topcon TRC NW6) at  $45^\circ$  FOV with a resolution of  $1440 \times 960$ ,  $2240 \times 1488$  or  $2304 \times 1536$  pixels and are stored in TIFF format. Out of 1200 images 800 are captured with pupil dilation. The reference standard provided contains the grading for diabetic retinopathy and the risk of macular edema in each image.

#### 2.3.6. Review

The Retinal Vessel Image set for Estimation of Widths (REVIEW) [25] was made available online in 2008 by the Department of Computing and Informatics at the University of Lincoln, Lincoln, UK. The dataset contains 16 mydratic images with 193 annotated vessel segments consisting of 5066 profile points manually marked by three independent experts. The 16 images are subdivided into four sets, the high resolution image set (HRIS, 8 images), the vascular disease image set (VDIS, 4 images), the central light reflex image set (CLRIS, 2 images) and the kickpoint image set (KPIS, 2 images).

#### 2.3.7. ROC microaneurysm set

The ROC microaneurysm dataset [26] is part of a multi-year online competition of microaneurysm detection that was arranged by the University of Iowa in 2009. The database consists of 100 digital color fundus photographs containing microaneurysms and is subdivided into a training set of 50 images and a test set of 50 images. A reference standard indicating the location of microaneurysms is provided with the training set. The images are captured using either a TopCon NW100 or a Canon CR5-45NM camera at  $45^\circ$  FOV and was JPEG compressed in the camera. There are three different image sizes present in the database;  $768 \times 576$ ,  $1058 \times 1061$  and  $1389 \times 1383$  pixels.

#### 2.3.8. VICAVR database

The VICAVR database [27] is a set of retinal images used for the computation of the A/V ratio. The database currently includes 58 images. The images have been acquired with a TopCon non-mydratic camera NW-100 model and are optic disc centered with a resolution of  $768 \times 584$ . The database includes the caliber of the vessels measured at different radii from the optic disc as well as the vessel type (artery/vein) labeled by three experts.

### 2.4. Performance measures

In the retinal vessel segmentation process, the outcome is a pixel-based classification result. Any pixel is classified either as vessel or surrounding tissue. Consequently, there are four possibilities; two classifications and two misclassifications. The classifications are the true positive (TP) where a pixel is identified as vessel in both the ground truth and segmented image, and the true negative (TN) where a pixel is classified as a non-vessel in the ground truth and the segmented image. The two misclassifications are the false negative (FN) where a pixel is classified as non-vessel in the segmented image but as a vessel pixel in the ground truth image, and the false positive (FP) where a pixel is marked as vessel in the segmented image but non-vessel in the ground truth image.

The true positive rate (TPR) represents the fraction of pixels correctly detected as vessel pixels. The false positive rate (FPR) is the fraction of pixels erroneously detected as vessel pixels. The accuracy (Acc) is measured by the ratio of the total

**Table 1 – Performance metrics for retinal vessel segmentation.**

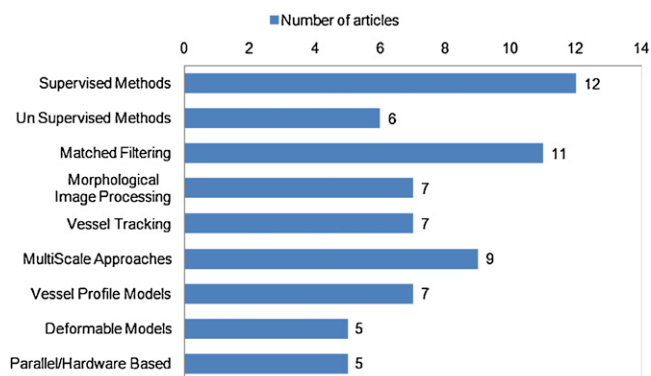
| Measure          | Description               |
|------------------|---------------------------|
| TPR              | TP/vessel pixel count     |
| FPR              | FP/non-vessel pixel count |
| Specificity (SP) | TN/(TN + FP)              |
| Sensitivity (SN) | TP/(TP + FN)              |
| Accuracy (Acc)   | (TP + TN)/FOV pixel count |

number of correctly classified pixels (sum of true positives and true negatives) to the number of pixels in the image field of view. Sensitivity (SN) reflects the ability of the algorithm to detect the vessel pixels. Specificity (SP) is the ability to detect non-vessel pixels. It can be expressed as  $1 - \text{FPR}$ . The positive predictive value (PPV) or precision rate gives the proportion of identified vessel pixels which are true vessel pixels. The PPV is the probability that an identified vessel pixel is a true positive.

A receiver operating characteristic (ROC) curve plots the fraction of vessel pixels correctly classified as vessel, namely the TPR, versus the fraction of non-vessel pixels wrongly classified as vessel, namely the FPR. The closer the curve approaches the top left corner; the better is the performance of the system. The most frequently used performance measure extracted from the ROC curve is the value of the area under the curve (AUC) which is 1 for an optimal system. For retinal images, the TPR and FPR are computed considering only pixels inside the FOV. Table 1 summarizes the performance metrics used by retinal vessel segmentation algorithms.

### 3. Classification of retinal vessel segmentation approaches

A common categorization of algorithms for segmentation of vessel like structures in medical images [15] includes image driven techniques, such as edge-based and region-based approaches; pattern recognition techniques, model-based approaches, tracking-based approaches and neural network-based approaches. In this review, we are dealing with vessel segmentation explicitly in two dimensional retinal images therefore, following the convention; the papers are categorized according to the image processing methodologies employed and the algorithms used. We have divided the retinal vessel segmentation algorithms into six main categories; (1) pattern recognition techniques, (2) matched filtering, (3) vessel tracking/tracing, (4) mathematical morphology, (5) multiscale approaches, (6) model based approaches and (7) parallel/hardware based approaches. Some of these categories are further divided into subcategories. Each segmentation method category is introduced, discussed and the papers of this category are summarized. The performance measures used by the segmentation algorithms are tabulated at the end of each section. Moreover, a table allowing a qualitative comparison of methods is also provided at the end of each section which includes the input image type, the image database used for evaluation, the quantitative performance measure used to evaluate the algorithm, whether the method is automated or involves human interaction, whether the algorithm deals with noisy retinal images, whether pathologies in the

**Fig. 4 – Categorization of articles by vessel segmentation methodology.**

retina are taken into account by the algorithm and finally, whether the algorithm particularly handles the central vessel reflex problem or not. In this survey, a total of 69 papers have been selected from peer-reviewed publications. The reviewed papers are summarized in Table 2 on the basis of the image processing technique used for segmentation. The fourth column illustrates the performance metrics used to evaluate the algorithm. The penultimate column indicates that the algorithm's capability to handle noisy images, pathological images and images containing central vessel reflex. "Nse", "Pth" and "Cvr" values in this column indicate that algorithm is capable of handling the noisy, pathological and central vessel reflex images, respectively.

Fig. 4 shows the frequency of the distribution of articles to various segmentation approaches. It illustrates that of these reviewed articles, 17% use supervised methods for pixel classification, 9% employ unsupervised pattern classification techniques and 16% adopt matched filtering techniques. The methodologies based on vessel tracking and mathematical morphology is espoused by 10% and 10% of articles, respectively. About 13% of articles follow multi-scale approaches and 17% are based on model based approaches. Around 7% of selected algorithms are implemented using parallel hardware based approaches.

The computerized understanding of the ocular fundus dates back to 1982 [28] and the first paper on retinal vessel segmentation appears in 1989 by Chaudhuri et al. [46]. Out of 69 selected articles, 13 were published by the year of 2000. The year-wise publication of selected articles is shown in Fig. 5. There were three publications in the year of 2001 followed by two, and five in the years of 2002–2003 and 2004, respectively. Five articles were published in the years of 2005–2006. The number of articles increased to eleven in the 2007. Seven articles per year were published in 2008 and 2009 followed by a considerable increase in the year of 2010 to 12 articles followed by four as of September 2011.

#### 3.1. Pattern classification and machine learning

The algorithms based on pattern recognition deal with the automatic detection or classification of retinal blood vessel features and other non vessel objects including background. Pattern recognition techniques for vessel segmentation are

**Table 2 – Categorization retinal vessel segmentation methods.**

| Algorithm                       | Year | Image processing technique   | Performance metrics | Nse/Pth/Cvr | Section                                     |                                |
|---------------------------------|------|--|---------------------|-------------|---|--------------------------------|
| Akita and Kuga [28]             | 1982 | Artificial neural networks   | Visual              | No          | Supervised classification methods (3.1.1)   |                                |
| Nekovei and Ying [29]           | 1995 | Back propagation neural network  | Visual              | No          |   |                                |
| Sinthanayothin et al. [30]      | 1999 | Principal Component Analysis and neural network                                  | SN, SP              | No          |   |                                |
| Abramoff et al. [31]            | 2004 | Gaussian derivative and k-NN classifier  | Acc, AUC            | No          |   |                                |
| Staal et al. [32]               | 2004 | Image ridges and k-NN classifier   | Acc, AUC            | No          |   |                                |
| Soares et al. [33]              | 2006 | Gabor filter and Gaussian mixture model (GMM) classifier                         | Acc, AUC            | No          |   |                                |
| Ricci and Perfetti [34]         | 2007 | Line operator and Support Vector Machine (SVM)                                   | Acc, AUC            | Nse/Cvr     |   |                                |
| Osareh and Shadgar [35]         | 2009 | Multiscale Gabor filter and GMM classifier                                       | SN, SP, Acc, AUC    | No          |   |                                |
| Xu and Luo [36]                 | 2010 | Wavelets, Hessian matrix and SVM   | SN, Acc             | No          | Unsupervised classification methods (3.1.2) |                                |
| Lupascu et al. [37]             | 2010 | Feature based AdaBoost classifier  | SN, Acc, AUC        | No          |   |                                |
| You et al. [38]                 | 2011 | Radial projection and semi-supervised classification using SVM                   | SN, SP, Acc         | No          |   |                                |
| Marin et al. [39]               | 2011 | Gray level and moment invariant based features with neural network               | SN, SP, Acc, AUC    | Nse/Pth/Cvr |   |                                |
| Tolias and Panas [40]           | 1998 | Fuzzy C-means clustering   | Visual              | No          |   |                                |
| Ng et al. [41]                  | 2010 | Maximum likelihood estimation of scale space parameters                          | TPR, FPR            | No          |   |                                |
| Simó and de Ves [42]            | 2001 | Bayesian image analysis and statistical parameter estimation                     | Visual, TPR, FPR    | No          |   |                                |
| Kande et al. [43]               | 2009 | Spatially weighted fuzzy C-means clustering                                      | AUC                 | Pth         |   |                                |
| Salem et al. [44]               | 2007 | RADIUS based Clustering ALgorithm (RACAL)  | SN, SP              | No          | Matched filtering (3.2)                     |                                |
| Villalobos-Castaldi et al. [45] | 2010 | Local entropy and co-occurrence matrix (GLCM)                                    | SN, SP, Acc         | No          |   |                                |
| Chaudhuri et al. [46]           | 1989 | Two-dimensional Gaussian matched filter(MF)                                      | Acc, AUC            | No          |   |                                |
| Hoover et al. [21]              | 2000 | MF and threshold probing   | SN, SP, Acc         | No          |   |                                |
| Kochner et al. [47]             | 1998 | Steerable filters  |                     | No          |   |                                |
| Gang et al. [48]                | 2002 | Amplitude modified second order Gaussian filter                                  | Visual              | No          |   |                                |
| Xiaoyi and Mojon [49]           | 2003 | Verification based multi threshold probing                                       | Acc, AUC            | No          |   |                                |
| Al-Rawi et al. [50]             | 2007 | Improved Gaussian matched filter   | Acc, AUC            | No          |   |                                |
| L. Sukkaew et al. [51]          | 2007 | Statistically optimized Laplacian Of Gaussian, skeletonization                   | SN, SP              | Nse         |   |                                |
| Yao and Chen [52]               | 2009 | Gaussian MF and Pulse coupled neural network                                     | TPR, FPR            | No          |   |                                |
| Cinsdikici and Aydin [53]       | 2009 | Matched filter and ANT colony algorithm  | SN, SP, Acc         | No          |   |                                |
| Zhang et al. [54]               | 2010 | Gaussian matched filter in combination with first order derivative.              | Acc, AUC            | No          |   |                                |
| Amin and Yan [55]               | 2010 | Phase Concurrency and log-Gabor filter   | TPR, FPR            | No          |   |                                |
| Zana and Klein [56]             | 2001 | Morphological processing and cross curvature evaluation                          | TPR, Acc, AUC       | Nse         |   | Morphological processing (3.3) |
| Ayala et al. [57]               | 2005 | Fuzzy mathematical morphology  | TPR, FPR            | No          |   |                                |
| Mendonca and Campilho [58]      | 2006 | Difference of Offset Gaussian filter and multiscale morphological reconstruction | Acc, AUC            | No          |   |                                |
| Yang et al. [59]                | 2008 | Mathematical morphology and fuzzy clustering                                     | Visual              | No          |   |                                |

|                            |      |  |                            |         |  |
|----------------------------|------|--|----------------------------|---------|--|
| Sun et al. [60]            | 2010 | Multiscale morphology, fuzzy filter and watershed transformation             | Visual                     | No      |  |
| Fraz et al. [61]           | 2011 | Vessel centerline detection and morphological bit-plane slicing.             | TPR, FPR, SN, SP, Acc, PPV | No      |  |
| Miri and Mahloojifar [62]  | 2011 | Curvelet transform and multi-structure elements morphology by reconstruction | TPR, FPR, Acc              | Nse     |  |
| Liu and Sun [63]           | 1993 | Adaptive tracking  | Visual                     | No      | Vessel tracing/tracking (3.4)                |
| Liang et al. [64]          | 1994 | Matched filter based iterative tracking with manual intervention             | Visual                     | No      |  |
| Chutatape et al. [65]      | 1998 | Gaussian and Kalman filters  | Visual                     | No      |  |
| Quek and Kirbas [66]       | 2001 | Wave propagation and traceback   | Visual                     | Nse     |  |
| Ali et al. [67]            | 1999 | Recursive tracking with directional templates                                | Visual                     | No      |  |
| Kelvin et al. [68]         | 2007 | Optimal contour tracking   | Acc                        | Nse     |  |
| Delibasis et al. [69]      | 2010 | Model based tracing  | SN, SP, Acc                | No      |  |
| Frangi et al. [70]         | 1998 | Eigen decomposition of Hessian and Frobenius Norm                            | Visual                     | No      | Multiscale approaches (3.5)                  |
| Martinez-Perez et al. [71] | 1999 | Scale space analysis of maximum principal curvature                          | Visual                     | No      |  |
| Martinez-Perez et al. [72] | 2007 | Maximum principal curvature, gradient magnitude and region growing           | TPR, FPR, Acc              | No      |  |
| Perez et al. [73]          | 2007 | ITK serial implementation  | TPR, FPR, Acc              | No      |  |
| Wink et al. [74]           | 2004 | Vector valued multiscale representation                                      | Visual                     | Nse     |  |
| Sofka and Stewart [75]     | 2006 | Likelihood ratio test with confidence and edge measures                      | Visual                     | Nse/Pth |  |
| Anzalone et al. [76]       | 2008 | Scale space analysis and parameter search                                    | TPR, FPR, Acc              | No      |  |
| Farnell et al. [77]        | 2008 | Multiscale Line Operator and region growing.                                 | AUC                        | No      |  |
| Vlachos and Dermatas [78]  | 2009 | Multiscale line tracking   | SN, SP, Acc                | Nse     |  |
| Vermeer et al. [79]        | 2004 | Laplacian profile model  | SN, SP                     | C       | Vessel profile models (3.6.1)                |
| Mahadevan et al. [80]      | 2004 | Vessel profile model   | Visual                     | Nse/Pth |  |
| Li et al. [81]             | 2007 | Multiresolution Hermite model  | SN, SP                     | Nse/Cvr |  |
| Lam and Hong [82]          | 2008 | Divergence of vector fields  | Acc, AUC                   | Nse/Pth |  |
| Lam et al. [83]            | 2010 | Multiconcavity modeling  | Acc, AUC                   | Nse/Pth |  |
| Narasimha-Iyer et al. [84] | 2007 | Dual Gaussian profile model  | Visual                     | Nse/Cvr |  |
| Zhu [85]                   | 2010 | Log-Gabor filters, phase concurrency and Fourier domain                      | Visual                     | Nse     |  |
| Espona et al. [86]         | 2007 | Snakes in combination with blood vessel topological properties               | SN, SP, Acc                | No      | Deformable models (3.6.2)                    |
| Espona et al. [87]         | 2008 | Snakes in combination with morphological processing                          | SN, SP, Acc                | No      |  |
| Al-Diri et al. [88]        | 2009 | Ribbon of Twin active contour model  | SN, SP                     | Cvr     |  |
| Sum and Cheung [89]        | 2008 | Chan-Vese contour model  | Visual                     | Nse     |  |
| Zhang et al. [90]          | 2009 | Nonlinear projections, variational calculus                                  | TPR, FPR, Acc              | No      |  |
| Alonso-Montes et al. [91]  | 2005 | Cellular Neural Network (CNN) based algorithm                                | Visual                     | No      | Parallel hardware based implementation (3.7) |
| Alonso-Montes et al. [92]  | 2008 | Pixel level snakes, pixel-parallel approach                                  | Acc                        | No      |  |
| Renzo et al. [121]         | 2007 | CNN with virtual template expansion  | Acc, AUC                   | No      |  |
| Costantini et al. [122]    | 2010 | CNN with virtual template expansion  | Acc, AUC                   | No      |  |
| Palomera-Perez et al. [93] | 2010 | ITK parallel implementation  | TPR, FPR, Acc              | No      |  |

Performance metrics: visual–visual comparison, SN – sensitivity, SP – specificity, Acc – accuracy, AUC – area under curve. Nse/Pth/Cvr *Images* means noisy images/pathological images/central vessel reflex images. “Nse”, “Pth” and “Cvr” values in this column indicate that algorithm is capable of handling the noisy, pathological and central vessel reflex images, respectively.

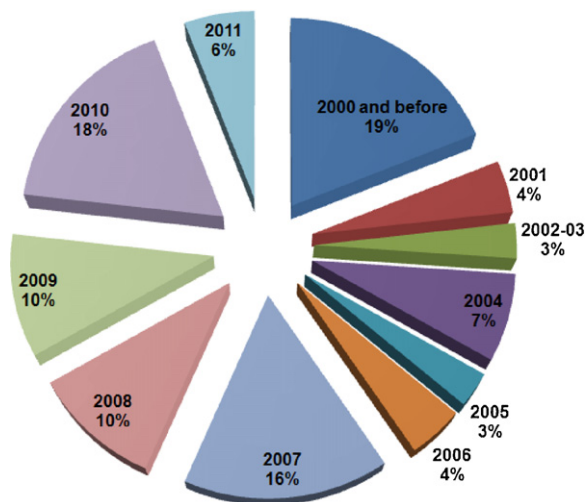


Fig. 5 – Yearly decomposition of reviewed articles.

divided into two categories; supervised approaches and unsupervised approaches. Supervised methods exploit some prior labeling information to decide whether a pixel belongs to a vessel or not, while unsupervised methods perform the vessel segmentation without any prior labeling knowledge.

### 3.1.1.1. Supervised methods

In supervised methods, the rule for vessel extraction is learned by the algorithm on the basis of a training set of manually processed and segmented reference images often termed as the gold standard. This vascular structure in these ground truth or gold standard images is precisely marked by an ophthalmologist. However, as noted by Hoover et al. [21] there is significant disagreement in the identification of vessels even amongst expert observers. In a supervised method, the classification criteria are determined by the ground truth data based on given features. Therefore the prerequisite is the availability of the already classified ground truth data, which may not be available in real life applications. As supervised methods are designed based on pre-classified data, their performance is usually better than that of unsupervised ones and can produce very good results for healthy retinal images.

Artificial neural networks have been extensively investigated for segmenting retinal features such as the vasculature [28] making classifications based on statistical probabilities rather than objective reasoning. These neural networks employ mathematical weights to decide the probability of input data belonging to a particular output. This weighting system can be adjusted by training the network with data of known output typically with a feedback mechanism to allow retraining.

Nekovei and Ying [29] describe an approach using a back-propagation network for the detection of blood vessels in angiography. The method applies the neural network directly to the angiogram pixels without prior feature detection. The pixels of the small sub-window, which slides across the angiogram image, are directly fed as input to the network. The feature vectors are formed by gray-scale values from the sub window centered on the pixel being classified. The ground truth images of manually labeled angiograms are used as the

training set to set the network's weights. A modified version of the common delta-rule is used to obtain these weights.

The use of principal component analysis (PCA) followed by neural networks is demonstrated by Sinthanayothin et al. [30] for localization of anatomical structures in retinal images. They reported a success rate of 99.56% for the training data and 96.88% for the validation data, respectively, with an overall sensitivity and specificity of 83.3% (standard deviation 16.8%) and 91% (standard deviation 5.2%), respectively. The result of the approach was compared with an experienced ophthalmologist manually mapping out the location of the blood vessels in a random sample of seventy three  $20 \times 20$  pixel windows and requiring an exact match between pixels in both images. Niemeijer [31] extracts a feature vector for each pixel that consists of the green plane of the RGB image and the responses of a Gaussian matched filter and its first and second order derivatives at the scales of 1, 2, 4, 8, 16 pixels. Afterwards the  $k$ -Nearest Neighbor ( $k$ -NN) algorithm [94] is employed to estimate the probability of the pixel belonging to a vessel. The binary vasculature structure is obtained by thresholding the probability map. The algorithm is tested on the DRIVE database resulting in an average accuracy of 0.9416 and area under the ROC curve of 0.9294.

Staal [32] presented a ridge based vessel segmentation methodology from colored images of the retina which exploits the intrinsic property that vessels are elongated structures. The technique is based on an extraction of image ridges, which are natural indicators of vessels and coincide approximately with vessel centerlines. Image primitives are computed by grouping the ridge pixels into the sets that approximate straight line elements. The image is partitioned into convex set regions by assigning each image pixel to the closest line element from these sets. Every line element defines a local coordinate frame within each patch, in which local features are extracted for every pixel. In total, 27 features are selected from convex set regions, collectively as well as from individual pixels, using a sequential forward selection method. A  $k$ -NN classifier is used for classification. The methodology is tested on the publicly available STARE and Utrecht database obtained from a screening programme in the Netherlands. The method achieves an average accuracy of 0.9516 and an area under the ROC curve of 0.9614 on the STARE database.

The use of a 2-D Gabor wavelet and supervised classification for retinal vessel segmentation has been demonstrated by Soares et al. [33]. Each pixel is represented by a feature vector composed of the pixel's intensity and two-dimensional Gabor wavelet transform responses taken at multiple scales. A Gaussian mixture model classifier (a Bayesian classifier in which each class-conditional probability density function is described as a linear combination of Gaussian functions) is used to classify each pixel as either a vessel or non-vessel pixel. The methodology is evaluated on the DRIVE and STARE datasets resulting in an average accuracy of 0.9466 and 0.9480 and the area under the ROC curve as 0.9614 and 0.9671 for DRIVE and STARE, respectively. The algorithm takes in to account the information local to each pixel through image filters, ignoring useful information from shapes and structures present in the image. It does not work very well on the images with non uniform illumination as it produces false

detection in some images on the border of the optic disc, hemorrhages and other types of pathologies that present strong contrast.

The application of line operators as feature vector and SVM for pixel classification is proposed by Ricci and Perfetti [34]. A line detector which is based on the evaluation of the average grey level along lines of fixed length passing through the target pixel at different orientations is applied to the green channel of an RGB image and the response is thresholded to obtain unsupervised pixel classification. Moreover, two orthogonal line detectors are also employed along with the grey level of the target pixel to construct a feature vector for supervised classification using a support vector machine. With respect to other supervised techniques, the algorithm (1) requires fewer features, (2) feature extraction is computationally simpler, and (3) fewer examples are needed for training. The algorithm makes use of local differential computation of the line strength which makes the line detector robust with respect to non-uniform illumination and contrast. Also the line detector behavior in the presence of a central reflex is satisfactory. The performance of both methods is evaluated on the publicly available DRIVE and STARE databases through ROC analysis, resulting in average accuracy of 0.9563 and 0.9584 and the area under ROC curve as 0.9558 and 0.9602 for DRIVE and STARE, respectively.

Osareh and Shadgar [35] use multiscale Gabor filters for vessel candidate identification, then the features are extracted using principal component analysis. The parameters for Gabor filters are optimally tuned with experimentations. The image pixels are classified as vessels and non-vessels using the corresponding feature vectors by the Gaussian mixture model (GMM) and support vector machines (SVM). The methodology is tested on DRIVE as well as on the author's dataset consisting of 90 normal and abnormal images. The classification accuracy obtained is 95.24%, with 96.14% sensitivity and 94.84% specificity with the GMM. The best overall accuracy, using optimal parameters for SVM is 96.75% with 96.50% sensitivity and 97.10% specificity. The methodology achieves area under the ROC curve as 0.965 on the DRIVE database. However, there are some false positives due to background noise and non-uniform illumination, the border of the optic disc and other types of pathologies and the thinnest vessels are also not detectable, however, these thin vessels are not of much clinical importance.

The combination of several image processing techniques with SVM classification for vessel segmentation is proposed by Xu and Luo [36]. The background of the green channel is normalized, the large vessels are segmented using adaptive local thresholding and the optic disc edges are removed. The original image is then processed by wavelets at multiple scales for feature extraction. The line detectors are used to identify thin vessels. A 12 dimensional feature vector for each residual pixel in the binary retinal image excluding large vessels is constructed and an SVM is used to distinguish thin vessel segments from all the fragments. A tracking method based on a combination of vessel direction and the eigenvector of the Hessian matrix is used for thin vessel growth to obtain a segmented vessel tree. The method achieves an average accuracy of 0.9328 and an average sensitivity of 0.7760 on the DRIVE database.

Lupascu et al. [37] introduces another supervised method known as the feature-based AdaBoost classifier (FABC) for vessel segmentation. The 41-D feature vector is a rich collection of measurements at different spatial scales ( $\sqrt{2}$ , 2,  $2\sqrt{2}$  and 4), including the output of various filters (Gaussian and derivatives of Gaussian filters, matched filters, and 2-D Gabor wavelet transform), and the likelihood of structures like edges and ridges via numerical estimation of the differential properties of the intensity surface (principal and mean curvatures, principal directions, and root mean square gradient). This feature vector encodes a rich description of vessel-related image properties, namely local (pixel's intensity and Hessian-based measures), spatial (e.g., the gray-level profile of the cross section of a vessel can be approximated by a Gaussian curve) and structural (e.g., vessels are geometrical structures, which can be seen as tubular). An AdaBoost classifier is trained on 789,914 gold standard examples of vessel and non vessel pixels. The method achieves an average accuracy of 0.9597, an area under the ROC curve of 0.9561 and a kaapa measure of 0.72 on the DRIVE dataset. The strength of FABC lies in its capturing a rich collection of shape and structural information, in addition to local information at multiple spatial scales, in the feature vector. FABC does not discuss the issues related to the connection of broken vessel segments and some local ambiguities present due to the convergence of multiple and variously bent vessels.

The combination of the radial projection and the semi-supervised self-training method using SVM is employed by You et al. [38] for vessel segmentation. The vessel centerlines and the narrow and low contrast blood vessels are located using radial projections. A modified steerable complex wavelet is employed for vessel enhancement. The line strength measures are applied to the vessel enhanced image to generate the feature vector. The SVM classifier is used in a semi-supervised self training to extract the major structure of vessels. The segmented vasculature is obtained by the union of the two. The algorithm self learns from human-labeled data and weakly labeled data therefore yielding good results with decrease in the detection of false vessels. The method is very good in detecting narrow and low contrast vessels but prone to errors in case of pathologies. The average accuracy, sensitivity and specificity on the DRIVE database is 0.9434, 0.7410, and 0.9751, respectively and for the STARE database 0.9497, 0.7260, and 0.9756, respectively.

Marin et al. [39] presented a neural network based supervised methodology for the segmentation of retinal vessels. The methodology uses a 7-D feature vector composed of gray-level and moment invariant-based features. A multilayer feed forward neural network is utilized for training and classification. The input layer consists of seven neurons, the three hidden layers consist of fifteen neurons each and output layer is comprised of single neuron. The method proves to be effective and robust with different image conditions and on multiple image databases even if the neural network is trained on only one database. The average accuracy, AUC, sensitivity and specificity on the DRIVE database is 0.9452, 0.9588, 0.7067, and 0.9801, respectively and for the STARE database 0.9526, 0.9769, 0.6944, and 0.9819, respectively.

The performance measures adopted for evaluating the efficiency of supervised classification of retinal vessels are illustrated in Table 3, where on evaluation according to

**Table 3 – Performance measures for supervised methods.**

| Methodology                | Database      | Sensitivity | Specificity | Accuracy | Area under ROC |
|----------------------------|---------------|-------------|-------------|----------|----------------|
| Human observer             | DRIVE         | 0.7763      | 0.9723      | 0.9470   | –              |
|                            | STARE         | 0.8951      | 0.9384      | 0.9348   | –              |
| Sinthanayothin et al. [30] | Local dataset | 0.833       | 0.91        | –        | –              |
| Abramoff et al. [31]       | DRIVE         | 0.7145      | –           | 0.9416   | 0.9294         |
| Staal et al. [32]          | DRIVE         | –           | –           | 0.9442   | 0.952          |
|                            | STARE         | –           | –           | 0.9516   | 0.9614         |
| Soares et al. [33]         | DRIVE         | –           | –           | 0.9466   | 0.9614         |
|                            | STARE         | –           | –           | 0.9480   | 0.9671         |
| Ricci and Perfetti [34]    | DRIVE         | –           | –           | 0.9563   | 0.9558         |
|                            | STARE         | –           | –           | 0.9584   | 0.9602         |
| Osareh and Shadgar [35]    | DRIVE         | –           | –           | –        | 0.9650         |
| Lupascu et al. [37]        | DRIVE         | 0.72        | –           | 0.9597   | 0.9561         |
| Xu and Luo [36]            | DRIVE         | 0.7760      | –           | 0.9328   | –              |
| You et al. [38]            | DRIVE         | 0.7410      | 0.9751      | 0.9434   | –              |
|                            | STARE         | 0.7260      | 0.9756      | 0.9497   | –              |
| Marin et al. [39]          | DRIVE         | 0.7067      | 0.9801      | 0.9452   | 0.9588         |
|                            | STARE         | 0.6944      | 0.9819      | 0.9526   | 0.9769         |

accuracy, the AdaBoost classifier [37] as previously discussed, is shown to outperform the other compared algorithms.

### 3.1.2. Unsupervised methods

The approaches based on unsupervised classification attempt to find inherent patterns of blood vessels in retinal images that can then be used to determine that a particular pixel belongs to vessel or not. The training data or hand labeled ground truths do not contribute directly to the design of the algorithm in these approaches.

Tolias and Panas [40] develop a fuzzy C-means (FCM) clustering algorithm that uses linguistic descriptions like *vessel* and *non-vessel* to track fundus vessels in retinal angiogram images. The fuzzy vessel tracking process is based on finding the membership functions of the two linguistic values. First, the optic nerve and its bounding circle, which is a salient image region in fundus images, is detected and used as the starting point of the algorithm. Then, the FCM algorithm is applied to segment the points in the bounding circle as vessel and non-vessel. Each segmented region which contains more than three vessel points is considered as a candidate starting point of an iterative fuzzy vessel tracking algorithm. False candidate vessels are rejected by the algorithm within two or three iterations. The striking features of the algorithm are that is that it does not utilize any edge information to locate the exact location of the vessels and this reduces the effects of noise in the tracking procedure. Also, the algorithm uses only fuzzy image intensity information and makes no assumptions for the shape model of the vessels. Moreover no parametric tuning and initialization is needed. The algorithm resulted in good tracking of well-defined vessels in the image and missed only vessels of small diameter and low contrast.

The Bayesian image analysis for the segmentation of arteries, veins and the fovea in the retinal angiograms is employed by Simo and de Ves [42]. The segmentation task is formulated as the statistical parameter estimation by considering the input image “y” as a noisy version of the segmented image “x”

therefore considering it is as a parameter of the input image. The goal is to looking for the estimation of “x” as a parameter of “y” distribution. The stochastic model for the observed spatial intensities is based on a Gaussian noise process which is assumed to be statically independent between the pixels. The information about the anatomy of a fundus is incorporated by means of Markov random fields’ prior probability model. The segmented image “x” is estimated by simulated annealing and iterated conditional mode. The methodology is tested on various ocular fundus images and proved to be robust against added salt and pepper noise.

Salem et al. [44] proposed a Radius based Clustering Algorithm (RACAL) which uses a distance based principle to map the distributions of the image pixels. A partial supervision strategy is combined with the clustering algorithm. The features used are the green channel intensity, the local maxima of the gradient magnitude, and the local maxima of the large eigenvalue calculated from Hessian matrix. The performance of RACAL algorithms is compared with *k*-NN and found to be better in the detection of small vessels. The methodology attains a specificity of 0.9750 and sensitivity of 0.8215 on the STARE database.

An unsupervised fuzzy based vessel segmentation approach, proposed by Kande et al. [43], uses the intensity information from red and green channels of the same retinal image to correct non-uniform illumination in color fundus images. Matched filtering is utilized to enhance the contrast of blood vessels against the background. Finally spatially weighted fuzzy C-means clustering followed by connected component labeling is used to identify the vascular tree structure. On the DRIVE and STARE databases, the methodology achieves an area under the ROC curve of 0.9518 and 0.9602, respectively.

Ng et al. [41] developed a vessel detection system based on a maximum likelihood inversion of a model of image formation. The authors applied second derivative Gaussian filters to an image at several scales, and the filter outputs are used to

infer the presence of vessels and their properties. A generative model using a Gaussian-profiled valley for the detection of blood vessels is proposed and corresponding filter outputs are calculated. The Gaussian model of noise is also proposed and the covariance of filter outputs to the isotropic noise is calculated. The image and noise models are incorporated into a maximum likelihood estimator to estimate model parameters. The system produces an estimate of the width, contrast, and direction of the blood vessel at each point in the image. It also produces likelihoods of the model with additive noise. These likelihoods are used in conjunction with the estimated vessel parameters to detect the vessel centerline. The vessel is marked by combining the centerline and the estimated width parameter. The methodology is evaluated in terms of true positive and false positive percentage compared with both of the manual segmentations from the STARE database. It approximates with the methodologies of threshold probing [21] and the RISA system [95].

The local entropy information in combination with the gray-level co-occurrence matrix (GLCM) is used by Villalobos-Castaldi et al. [45] for vessel segmentation. First, a matched filter is used to enhance the vessels followed by the computation of the GLCM, from which a statistical feature is calculated, to act as a threshold value. Later local entropy thresholding is employed to segment the vessel network. The method is evaluated on DRIVE and the results obtained for sensitivity, specificity, and accuracy are 0.9648, 0.9480 and 0.9759, respectively.

Table 4 depicts the performance measures reported by various methodologies of retinal vessel segmentation based on unsupervised classification, with a high accuracy reported by Villalobos-Castaldi et al. [45] using GLCM.

### 3.2. Matched filtering

Matched filtering for the detection of the vasculature involves a 2-D kernel with the retinal image. The kernel is designed to model a feature in the image at some unknown position and orientation, and the matched filter response (MFR) indicates the presence of the feature. The following three properties are exploited in order to design the matched filter kernel: vessels usually have a limited curvature and may be approximated by piecewise linear segments, the diameter of the vessels decrease as they move radially outward from the optic disk, the cross-sectional pixel intensity profile of these line segments approximates a Gaussian curve. The convolution kernel may be quite large and needs to be applied at several rotations resulting in a computational overhead. In addition, the kernel responds optimally to vessels that have the same standard deviation of the underlying Gaussian function specified by the kernel. As a consequence, the kernel may not respond to those vessels which have a different profile. The retinal background variation and presence of pathologies in the retinal image also increase the number of false responses because the pathologies can exhibit the same local attributes as the vessels. A matched filter response method is found effective when used in conjunction with additional processing techniques.

Chaudhuri et al. [46] proposed a two-dimensional linear kernel with a Gaussian profile for segmentation of the retinal

vessels. The profile of the filter is designed to match that of a blood vessel, which typically has a Gaussian or a Gaussian derivative shape curve. The kernel is rotated in 15° increments to fit into vessels of different orientations. The highest response of filter is selected for each pixel and is thresholded to provide a binary vessel image. Further post processing is then applied to prune and identify the vessel segments.

Steerable filters [96] i.e. a filter with arbitrary orientation can be synthesized from the linear combination of basis filters. This class of filters is not applied in many directions. Rather, it is applied in only two basic directions and the response is calculated in other directions from a combination of the responses from these two directions. This approach has the advantage of faster computation for a reasonable accuracy. An example of applying steerable filters to vessel enhancement is also given. This concept is further extended by Kochner et al. [47].

The methodology described by Hoover et al. [21] combines local and region-based properties of retinal blood vessels for segmentation using a threshold probing technique on a matched filter response image. The method analyzes the MFR image, formulated by Chaudhuri et al. [46], in pieces and applies thresholding with iterative probing for each pixel as vessel or non-vessel. At each iteration, the probing technique analyzes the region-based attributes of the pixels in the tested area and segments the pixels classified as vessels. Pixels that are not classified as vessels from probes are recycled for further probing. A unique feature of this method is that each pixel is classified using local and region-based properties. The method is evaluated using hand-labeled images and tested against basic thresholding of the MFR. As much as 15 times reduction of false positives over the basic MFR and up to 75% true positive rate has been reported.

The amplitude-modified second order Gaussian filter [48] has also been utilized for vessel detection. It proves that the vessel width can be measured in a linear relationship with the spreading factor of the matched Gaussian filter when the magnitude coefficient of the Gaussian filter is suitably assigned. The vessel width measurement not only provides the size of blood vessel but it is also useful for optimizing the matched filter to improve the successful rate of detection.

An adaptive local thresholding framework based on a verification-based multi-threshold probing scheme [49] has also been investigated for vessel detection. This includes application-dependent verification procedure which incorporates the domain-specific knowledge about blood vessels including curvilinear angle, width, contrast, and size. After verification, the image is probed with a number of thresholds and a segmented binary vascular tree is obtained by the union of the images resulting from probed thresholds followed by non maxima suppression based post processing techniques. The methodology works very well for healthy retinal images but is prone to increased false positive rates with pathological retinal images. The evaluation of the methodology resulted in an average accuracy of 0.9212 and an area under the ROC curve of 0.9114 on the publicly available DRIVE database.

An automated algorithm [51] for detection of the blood vessels in low quality and noisy retinal images of premature infants employs a statistically optimized LOG edge detection filter, Otsu thresholding, medial axis transform

**Table 4 – Performance measures for unsupervised methods.**

| Methodology                     | Database            | Sensitivity | Specificity | Accuracy | Area under ROC |
|---------------------------------|---------------------|-------------|-------------|----------|----------------|
| Human observer                  | DRIVE               | 0.7763      | 0.9723      | 0.9470   | –              |
|                                 | STARE               | 0.8951      | 0.9384      | 0.9348   | –              |
| Ng et al. [41]                  | STARE               | 0.7000      | 0.9530      | –        | –              |
| Kande et al. [43]               | DRIVE               | –           | –           | 0.8911   | 0.9518         |
|                                 | STARE               | –           | –           | 0.8976   | 0.9298         |
| Salem et al. [44]               | STARE               | 0.8215      | 0.9750      | –        | –              |
| Villalobos-Castaldi et al. [45] | DRIVE (without FOV) | 0.9648      | 0.9480      | 0.9759   | –              |

skeletonization followed by pruning, and edge thinning for vessel segmentation. The methodology is evaluated on 100 retinal images of premature infants and reported sensitivity and specificity of 0.9879 and 0.8934, respectively.

Al-Rawi et al. [50] improved Chaudhuri et al.'s [46] matched filter (MF) by using an exhaustive search optimization procedure on 20 retinal images of the DRIVE database to find the best parameters for matched filter size, the standard deviation and threshold value. The improved MF outperforms Chaudhuri's classical parameter matched filter.

Yao and Chen [52] uses a 2-D Gaussian matched filter for retinal vessel enhancement and then a simplified pulse coupled neural network [97] is employed to segment the blood vessels by firing neighborhood neurons. Next, a fast 2-D-Otsu algorithm is used to search the best segmentation results. Finally, the complete vessel tree is obtained via analyzing the regional connectivity. The evaluation on the STARE database indicates a 0.8035 true positive rate and a 0.0280 false positive rate.

A hybrid model of the matched filter and ANT colony algorithm [98] for retinal vessel segmentation is proposed by Cinsdikici and Aydin [53]. After some preprocessing, the image is passed through the matched filter and ANT algorithm in parallel. The results are then combined followed by length filtering to extract the complete vasculature. The algorithm is tested on the retinal images from the DRIVE database and optimal parameters are deduced. The algorithm achieved the area under the ROC as 0.9407 with an average accuracy of 0.9293 in 35 s average processing time. However, the algorithms mistakenly marked pathological areas as vessels and the segmented vessels are a little thicker than the manual marking.

The classical matched filter is generalized and extended [54] with the first-order derivative of the Gaussian (MF-FDOG) to exploit the property that for a blood vessel in the retina, the Gaussian shaped cross section is symmetric with respect to its peak position whereas the non-vessel edges, e.g. the step edge for lesions, are asymmetric. The methodology uses a pair of filters, the zero-mean Gaussian filter (MF) and the first-order derivative of the Gaussian (FDOG), to detect the vessels. For a true vessel, it will have a strong response to the MF around its peak position, while the local mean of its response to the FDOG will be close to zero around the peak position. In contrast, for non-vessel structures, for example the step edge, it will have a high response to the MF but the local mean of its response to the FDOG will also be high. The methodology achieves TPR, FPR and an accuracy of 0.7177, 0.0247 and 0.9484, respectively on STARE whereas for DRIVE, the measures are reported to be 0.7120, 0.0276 and 0.9382, respectively. The methodology

significantly reduces the false detections produced by the original MF and detects many fine vessels that are missed by the MF.

A high speed detection of retinal blood vessels using phase congruency has been proposed by Amin and Yan [55]. Initially phase congruency of the retinal image is generated which is a soft classification of vessels as well as invariant due to the change in image luminosity and contrast. A bank of log-Gabor filters are used for measuring phase congruency and a binary vessel tree is obtained by thresholding. The algorithm detects the vessels from images in the DRIVE and STARE databases in 10 s. The accuracy and area under the ROC curve is 0.92, 0.94 for DRIVE and 0.91, 0.92 for STARE, respectively. The comparison of selected performance measures for the methodologies based on matched filtering is illustrated in Table 5, where the highest accuracy is achieved by the improved matched filter method of Al-Rawi et al. [50].

### 3.3. Morphological processing

The word morphology commonly denotes a branch of biology that deals with the form and structures of animals and plants. The term mathematical morphology is used as a tool for extracting image components that are useful in the representation and description of region shapes such as features, boundaries, skeletons and convex hulls. The language of mathematical morphology is set theory and it offers a unified and powerful approach to numerous image processing problems. Morphological image processing [99] is a collection of techniques for digital image processing based on mathematical morphology. Morphological operators apply structuring elements (SE) to images, and are typically applied to binary images but can be extended to gray-level images. The two main morphological operators are *dilation* and *erosion*. *Dilation* expands objects by a defined Structuring Element, filling holes, and connecting the disjoint regions. *Erosion* shrinks the objects by a Structuring Element. The other two operations are *Closing*, which is a dilation followed by an erosion, and *Opening*, i.e. an erosion followed by a dilation. Two algorithms used in medical image segmentation and related to mathematical morphology are *top hat* and *watershed* transformations. The enhancement effect of a top-hat transformation is due to the estimation of local background by a morphology opening operation, which is subtracted from the original image resulting in enhanced vessels.

The basic morphology of the vasculature is known a priori to be comprised of connected linear segments. Morphological processing for identifying specific shapes has the advantage of

**Table 5 – Performance measures for the methods based on Matched Filtering.**

| Methodology               | Database | Sensitivity | Specificity | Accuracy | Area under ROC |
|---------------------------|----------|-------------|-------------|----------|----------------|
| Human observer            | DRIVE    | 0.7763      | 0.9723      | 0.9470   | –              |
|                           | STARE    | 0.8951      | 0.9384      | 0.9348   | –              |
| Chaudhuri et al. [46]     | DRIVE    | –           | –           | 0.8773   | 0.7878         |
| Hoover et al. [21]        | STARE    | 0.6751      | 0.9567      | 0.9267   | –              |
| Xiaoyi and Mojon [49]     | DRIVE    | –           | –           | 0.9212   | 0.9114         |
|                           | STARE    | –           | –           | 0.9337   | 0.8906         |
| Yao and Chen [52]         | STARE    | 0.8035      | 0.972       | –        | –              |
| Al-Rawi et al. [50]       | DRIVE    | –           | –           | 0.9535   | 0.9435         |
| Zhang et al. [54]         | DRIVE    | 0.7120      | 0.9724      | 0.9382   | –              |
|                           | STARE    | 0.7177      | 0.9753      | 0.9484   | –              |
| Cinsdikici and Aydin [53] | DRIVE    | –           | –           | 0.9293   | 0.9407         |
| Amin and Yan [55]         | DRIVE    | –           | –           | 0.92     | 0.94           |

speed and noise resistance. The main disadvantage of exclusively relying upon morphological methods is that they do not exploit the known vessel cross-sectional shape. In addition, the use of an overly long structuring element may cause difficulty in fitting to highly tortuous vessels.

The combination of morphological filters and cross-curvature evaluation to segment vessel-like patterns is employed by Zana et al. [8,56]. Mathematical morphology exploits the fact that the vessels are linear, connected and their curvature is varying smoothly along the crest line to highlight the vessels in the monochromatic retinal image. A cross-curvature evaluation is performed to identify the structures in a retinal image whose curvature is linearly coherent. The detection algorithm that derives directly from this model is based on four steps: (1) noise reduction, (2) linear pattern with Gaussian-like profile, (3) cross-curvature evaluation, (4) linear filtering. The algorithm had been tested on retinal photographs of three different types: fluoroangiograms, gray images obtained with a green filter, and color images with no filter. Occasionally a short preprocessing step was necessary since the algorithm only works with bright patterns in gray level images.

Ayala et al. [57] defines an average of fuzzy sets by making use of the average distance of Baddeley et al. [100] and the mean of Vorob'ev [101]. The segmentation procedures presented by [56], [46] and [3] have been revisited and modified using these new averages. All these procedures produce gray-scale images with enhanced blood vessels after low level processing. The threshold will be applied to this vessel enhanced image to generate a binary vessel tree. The authors retain the image obtained before applying the final threshold which is considered as a fuzzy set representing the vessels. For the Zana and Klein [56] method the segmentation result is heavily dependent on the length of the linear structuring element. A fuzzy set of structuring elements with varied length is defined and then the final result is obtained with the aggregation of a proposed fuzzy set average. The performance of the proposed technique is evaluated by defining a statistical measure for misclassification rates i.e. false positives and false negatives on two images from the STARE database and a decrease in the false positive rate is observed.

A Difference of Offset Gaussian (DoOG) filter in combination with multiscale morphological reconstruction [58] is utilized for retinal vasculature extraction. The vessel centerlines are extracted by applying the DoOG filter and the vessels are enhanced by applying a modified top hat operator with variable size circular structuring elements aiming at enhancement of vessels with different widths. The binary maps of the vessels are obtained at four scales by using morphological reconstruction with a double threshold operator. A final image with the segmented vessels is obtained by an iterative seeded region growing process of the centerline image with the set of four binary maps. The methodology is evaluated on two publicly available databases, the DRIVE database and the STARE database and resulted in the average accuracy of 0.9463 and 0.9440, respectively.

An automatic hybrid method comprising of the combination of mathematical morphology and a fuzzy clustering algorithm is presented by Yang et al. [59]. The blood vessels are enhanced and the background is removed with a morphological top-hat operation then the vessels are extracted by fuzzy clustering. The algorithm is tested on the STARE database and only visual comparisons are reported.

Sun et al. [60] combined morphological multiscale enhancement, fuzzy filter and watershed transformation for the extraction of the vascular tree in the angiogram. The background is estimated by using non linear multiscale morphology opening operators with a varying size of structuring element on each pixel and later subtracted from the image for contrast normalization. The normalized angiogram is processed by a combined fuzzy morphological operation with twelve linear structuring elements rotated every 15° between zero and 180°, with nine pixels length. The vessel region is obtained by thresholding the filtered image followed by a thinning operation to approximate the vessel centerlines. Finally, the vessel boundaries were detected using watershed techniques with the obtained vessel centerline. The algorithm is evaluated for the completeness and correctness of the extracted vascular tree from angiograms obtained from seven patients. The fuzzy filter is shown to be insensitive to the added Gaussian noise in the angiograms.

Fraz et al. [61] have proposed a unique combination of vessel centerlines detection and morphological bit plane slicing

to extract the blood vessel tree from the retinal images. The centerlines are extracted by using the first order derivative of a Gaussian filter in four orientations and then evaluation of derivative signs and average derivative values is performed. Mathematical morphology has emerged as a proficient technique for quantifying the blood vessels in the retina. The shape and orientation map of blood vessels is obtained by applying a multidirectional morphological top-hat operator with a linear structuring element followed by bit plane slicing of the vessel enhanced grayscale image. The centerlines are combined with these maps to obtain the segmented vessel tree. The methodology is tested on three publicly available databases DRIVE, STARE and MESSIDOR.

The fast discrete curvelet transform (FDCT) and multi-structure mathematical morphology [62] is employed for vessel detection. FDCT is used for contrast enhancement and the edges of blood vessels are detected by applying a multi-structure morphological transformation. The false edges are removed by morphological opening by reconstruction. An adaptive connected component analysis is performed for length filtering of the detected vascular structures in order to obtain a complete vascular tree. The method achieves an accuracy of 0.9458 with 0.7352 and 0.0205 TPR and FPR, respectively on the DRIVE database. Table 6 summarizes the results of various morphological image processing based retinal vessel segmentation techniques evaluated on the DRIVE and STARE databases. A high accuracy is reported by Mendoca and Campilho [58] when applied to the DRIVE dataset.

### 3.4. Vessel tracing/tracking

Vessel tracking algorithms segment a vessel between two points using local information and work at the level of a single vessel rather than the entire vasculature. The centre of the longitudinal cross-section of a vessel is determined with various properties of the vessel including average width gray level intensity and tortuosity measured during tracking. Tracking consists of following vessel center lines guided by local information, usually trying to find the path which best matches a vessel profile model. The main advantage of vessel tracking methods is that they provide highly accurate vessel widths, and can provide information about individual vessels that is usually unavailable using other methods. Noting that vessels are connected in the retina, these systems can follow a whole tree without wasting time examining the vast majority of the image that does not contain vessel. Vessel tracking can thus give information on vessel structure such as branching and connectivity. There are some complications relating to the technique that include the vessel tracking algorithms being unable to detect vessels or vessel segments which have no seed points and in addition, missing any bifurcation points can result in undetected sub-trees.

Generally, the vessel tracking algorithms are used in conjunction with matched filters of morphological operators. Some modifications and improvements are also suggested in the literature to deal with the above mentioned problems. To deal with the problem of the central light reflex area, [102] supposed the vessel intensity profiles can be modeled as twin Gaussian functions.

Adaptive tracking [63] is presented detection of vasculature in retinal angiograms, where the local vessel trajectories are estimated after giving an initial point within a vessel. Once a segment has been tracked, it is deleted in the angiogram image by growing the deletion intensity value over the gray levels representing the vessel. This procedure is performed recursively to extract the vascular tree. This algorithm also requires the user to specify vessel starting points.

Liang et al. [64] developed an algorithm to find the course of the vessel centerline and measure the diameter and tortuosity of a single vessel segment, although only diameter measurements are reported. The tracking of a blood vessel moves on by broadening the search in the direction of the last-tracked part of the blood vessel by a certain fixed length. The density profile on the perpendicular line in the extended direction is taken and a Gaussian matched filter is convolved with it and the result is examined. The strategy is to estimate the next location based on the current location, observe the next actual location by the matched filter, correct the estimation and then re-estimate the next location and continue iteratively. Moreover, the matched filter helps to ignore small branches at a bifurcation point without any special handling, thus allowing the tracking process to follow one major branch continuously. However, the algorithm needs manual intervention for start and end points and definition of the tracking direction.

Chutatape et al. [65] uses a tracking strategy with Gaussian and Kalman filters for blood vessel detection in retinal images. The second order Gaussian matched filter is employed to estimate the vessel centerline midpoint and then the tracking process is started from the circumference of the optic disc. The Kalman filter is employed to estimate the next vessel segment location using not only the parameters of the current segment but all previous vessel segments as well, similar to tracking a flying object in a radar system. The branch detection methodology is employed during tracking for detection of vessel branches.

A wave propagation and traceback mechanism [66] is proposed for the extraction of the vasculature from retinal angiography images. Each pixel is labeled in an angiogram with the likelihood that the pixel is a vessel pixel by using a dual-sigmoidal filter thus a vessel-likelihood image is obtained. This likelihood image is used to compute a cost function in the form of refractive indexes and then a digital wave is propagated through the image from the base of the vascular tree. This wave washes over the vasculature, ignoring local noise perturbations. The wave travels faster through low refractive index (likely to be a vessel) pixels, and slower through high refractive index pixels. The vasculature is obtained by tracing the wave along the local normal to the waveform. Wave propagation and traceback allows the extraction of not only the individual vessels, but the vascular connection morphology as well. The algorithm is evaluated on a set of six neurovascular angiogram images and it successfully detects 106 vessels out of 110.

Ali et al. [67] describes a real time algorithm which is based on recursively tracking the vessels starting from initial seed-points, using directional templates. Each directional template is designed to give the maximum response for an edge oriented in a particular direction. Around each candidate vessel point, the templates are applied on either side of the point

**Table 6 – Performance measures for morphological processing methodologies.**

| Methodology                | Database | Sensitivity | Specificity | Accuracy | Area under ROC |
|----------------------------|----------|-------------|-------------|----------|----------------|
| Human observer             | DRIVE    | 0.776330    | 0.972314    | 0.947046 | –              |
|                            | STARE    | 0.895177    | 0.938422    | 0.934891 | –              |
| Zana and Klein [56]        | DRIVE    | 0.6971      | –           | 0.9377   | 0.8984         |
| Mendonca and Campilho [58] | DRIVE    | 0.7344      | 0.9764      | 0.9452   | –              |
|                            | STARE    | 0.6996      | 0.9730      | 0.9440   | –              |
| M.M. Fraz et al. [61]      | DRIVE    | 0.7152      | 0.9769      | 0.9430   | –              |
|                            | STARE    | 0.7311      | 0.9680      | 0.9442   | –              |
| Miri and Mahloojifar [62]  | DRIVE    | 0.7352      | 0.9795      | 0.9458   | –              |

at varying distances. The edges are marked at points that yield the maximum response for the templates. The algorithm takes a step in the direction of maximum response and the procedure is repeated at the new point. Retinal features such as branching and cross-over points of the vessels are estimated by this algorithm once the vessels are segmented. This algorithm is very fast and prioritized versions have been used for real time feature extraction and registration at frame rates of 30 frames/s. The methodology is evaluated on healthy and pathological dilated retinal images captured using a TOPCON TRC-510A fundus camera using red-free illumination, and a Kodak Megaplus 1.4 CCD sensor attached to the top with a resolution of  $1024 \times 1024$  and the segmentation results are visually analyzed. For dealing with the problem of real time extraction of crossing and bifurcation of retinal vessels, Hong [103] describes an optimal algorithm to schedule the vascular tracing computations. A heuristic estimate of the optimal schedule is developed and used to guide the design of realizable scheduling algorithms.

A semi-automated method for the segmentation of vascular images is proposed by Kelvin et al. [68]. The method incorporates the multiscale vesselness filtering [70] into the conventional Livewire framework [104] to efficiently compute optimal medial axes. Sparse seed points along the vessel boundary are determined and optimal contours connecting these points are found using Dijkstra's algorithm. The cost function incorporates Frangi's multiscale vesselness measure, vessel direction consistency, the edge evidence and the spatial and radius smoothness constraints. The methodology is evaluated by segmenting retinal images from the publicly available DRIVE database and its performance is quantified by analyzing the reproducibility, accuracy, and efficiency. The technique reduced the overall segmentation task time by 68.2%, had a similarity ratio of 0.772 (0.775 between manual), and was 98.2% reproducible.

Delibasis et al. [69] presented an automatic model-based tracing algorithm for vessel segmentation and diameter estimation. The algorithm utilizes a parametric model of a vessel composed of a "stripe" which exploits geometric properties for parameter definitions. A measure of match (MoM) is defined which quantifies the similarity between the model and the given image. The initialization of seed pixels for vessel tracking is done using a [70] multiscale vesselness filter and dividing the binary output in non overlapping square blocks and picking a random non-zero pixel as a seed. The vessel tracking is derived by identifying the best matching strip with the vessel by using the seed point, strip orientation, strip width and

the MoM. Following the termination of vessel tracking, the algorithm actively seeks vessel bifurcation, without user intervention. The vessel diameter is also recovered with the defined model using the strip width parameter therefore assuming linear dependency between vessel diameter and model width parameter. The model parameters are fine tuned by using six of twenty available images of the DRIVE database as a training set. The random initialization of seeds produces non-identical algorithmic evolution, therefore revealing the stochastic nature of algorithm. The obtained average and standard deviation of the sensitivity, specificity and accuracy of the vessel segmentation are reported on the DRIVE database as  $72.88 \pm 0.63$ ,  $95.05 \pm 0.35$  and  $93.11 \pm 0.34$ , respectively.

### 3.5. Multi-scale approaches

The width of a vessel decreases as it travels radially outward from the optic disk and such a change in vessel caliber is a gradual one. Therefore, a vessel is defined as a contrasted pattern with a Gaussian like shape cross-section profile, piecewise connected, and locally linear, with a gradually decreasing vessel width. Therefore the idea behind scale-space representation for vascular extraction is to separate out information related to the blood vessel having varying width at different scales.

Frangi et al. [70] examined the multiscale second order local structure of an image (Hessian) in the context of developing a vessel enhancement filter. A vesselness measure is obtained on the basis of the eigenvalue analysis of the Hessian which finds out the principal directions in which the local second order structure of the image can be decomposed, which directly gives the direction of smallest curvature along the vessel. Two gray-level invariant geometric ratios are defined on the basis of eigenvalues and the Frobenius norm matrix is computed. The final vesselness measure is defined using the geometric ratios, the eigenvalues and the Frobenius norm matrix. This measure is tested on two dimensional digital subtraction angiography (DSA) and three dimensional aortoiliac and cerebral magnetic resonance angiography (MRA) data. Its clinical utility is shown by the simultaneous noise and background suppression. Many of the multiscale algorithms are based on this vessel enhancement filter.

Martinez-Perez et al. [71] present a method based on scale-space analysis from which the width, size and orientation of retinal blood vessels is obtained by using two main geometrical features based upon the first and the second derivative of the intensity (edges and the maximum principal

curvature) along the scale-space, that give information about the topology of the image. An edge point is characterized by the magnitude of the gradient of the image and at the ridge point the intensity image has a local maximum in the direction for which the gradient of the image undergoes the largest change (largest concavity). The local maxima over scales of the magnitude of the gradient and the maximum principal curvature are used as two features in a region growing procedure. In the first stage, the growth is constrained to regions of low gradient magnitude together with spatial information about the 8-neighboring pixels. In the final stage this constraint is relaxed to allow borders between regions to be defined. The algorithm is tested on both red-free and fluorescein retinal images and shows promising results.

Based on the above mentioned scale space segmentation algorithm [71], a semi-automatic method to measure and quantify geometrical and topological properties of the retinal vascular tree is also described [95]. The procedure consists of a semi-automatic labeling of the skeleton trees followed by an automatic procedure for measurement of length, area, diameter and branching angle of vessels. This information is generated as tabulated data and is used for further clinical analysis. Several geometrical and topological indexes are extracted. The methods are validated by comparison with manual measurements and applied to a pilot study of ten normal and ten hypertensive subjects and differences between groups in the morphological properties are investigated.

An extension [72] of this scale space algorithm [71] is demonstrated by exploiting the observation that the intensity of an image is proportional to the amount of blood in the light path corresponding to the particular pixel during image capture. Therefore a diameter-dependent equalization factor is applied to the multiscale information. The methodology attains TPR 0.7506, FPR 0.0431 and average accuracy 0.9410 on STARE and 0.7246 0.0345, 0.9344 TPR, FPR and average accuracy, respectively on the DRIVE database.

The algorithm [71] is further improved in [73] by using the insight segmentation and registration toolkit (ITK) [105]. The ITK implementation attains TPR 0.779, FPR 0.0591 and average accuracy of 0.924 on STARE whereas the TPR, FPR and average accuracy for DRIVE are 0.660, 0.038 and 0.922, respectively.

Wink et al. [74] have developed a method for central axis extraction that finds a minimum cost path using the vector-valued multiscale representation of a feature. First, a representation of a vessel segment at different scales is constructed using Eigen decomposition of the Hessian matrix, and then the vector-valued response image has to be converted to a 3-D cost-image to allow a minimum cost path search for a wave front propagation between two or more user defined points to retrieve the central axis of retinal vessels. The methodology is tested on synthetic and real angiograms and shows its potential to cope with severe stenosis or imaging artifacts in the image.

A likelihood ratio test [75] has been used for vessel centerlines extraction that combines matched-filter responses, confidence measures and vessel boundary measures. A multiscale matched filter for vessels is introduced to allow the combination of responses across scales to extract vessels with varying width. The filter response is augmented with a vessel confidence measure which is defined as a projection of a

vector formed from a normalized pixel neighborhood onto a normalized ideal vessel profile. Later, vessel boundary measures and associated confidences are computed at purported vessel boundaries. A six-dimensional measurement vector is obtained by combining the responses. A training technique is used to develop the “vesselness measure” which is actually a mapping of a 6-D feature vector to a single likelihood ratio. Finally, this vesselness likelihood ratio is used by a vessel tracing framework to produce the complete tree of vessel centerlines.

Anzalone [76] proposed a modular supervised algorithm for vessel segmentation in red-free retinal images. The image background is normalized for uneven illumination conditions followed by vessel enhancement using scale space theory. A supervised optimization procedure is used to determine the optimal scale factor and threshold for binarization of the segmented image followed by a cleaning operation for spur removal. The algorithm is tested on the DRIVE database and reported accuracy, TPR and FPR are 0.9419 0.7286 and 0.019, respectively.

The multiscale line operator (MSLO) [77] is also investigated for segmentation of retinal vessels. A Gaussian pyramid of sub-sampled images is constructed by using a series of images at consecutively coarser length scales via Gaussian sampling with respect to the original retinal image. The line operator is applied to the images on each level of the pyramid separately. The line-operator-filtered images on the coarser scales of the pyramid were mapped to the original (finest) level of scale by using a cubic spline. The final result is the sum of all images in the Gaussian pyramid and equal weighting is given to each length scale in the final MSLO image followed by a threshold to form a binary segmentation of the blood vessels. The noise in the binary image is removed by a simple region growing algorithm. This algorithm is evaluated on STARE and ARIA ([www.eyecharity.com/aria\\_online/](http://www.eyecharity.com/aria_online/)) databases and the reported AUC is 0.940 and 0.895, respectively.

Vlachos et al. [78] proposed a multi-scale line tracking for vasculature segmentation. After luminosity and contrast normalization, the seeds for line tracking are derived from a brightness selection rule from a normalized histogram. The line tracking is initialized at multiple scales to accommodate varying vessel widths. Several cross sectional profile conditions are defined for termination conditions for line tracking. The multi-scale confidence image map is derived after combining the results of multi-scale line tracking. The initial vessel network is derived after map quantization of the multi-scale confidence map. Median filtering is applied afterwards for restoration of disconnected vessel lines and eliminating noisy lines. Finally, post-processing removes erroneous artifacts using directional attributes of vessels and morphological reconstruction. The methodology is evaluated on the publicly available DRIVE database and attains the average accuracy of 0.929 with 0.747 of sensitivity and 0.955 of specificity. The methodology is very much dependent upon initial selection of seeds for line tracking.

The performance measures including TPR, FPR, sensitivity, specificity, accuracy and area under ROC curve for the methods based on multi-scale approaches are illustrated in Table 7, showing [71,72] the scale-space approach to achieve the

**Table 7 – Performance measures for multiscale approaches.**

| Methodology                | Database | Sensitivity | Specificity | Accuracy | Area under ROC |
|----------------------------|----------|-------------|-------------|----------|----------------|
| Human observer             | DRIVE    | 0.776330    | 0.972314    | 0.947046 | –              |
|                            | STARE    | 0.895177    | 0.938422    | 0.934891 | –              |
| Martinez-Perez et al. [71] | DRIVE    | 0.6389      | –           | 0.9181   | –              |
| Martinez-Perez et al. [72] | DRIVE    | 0.7246      | 0.9655      | 0.9344   | –              |
|                            | STARE    | 0.7506      | 0.9569      | 0.9410   | –              |
| Perez et al. [73]          | DRIVE    | 0.660       | 0.9612      | 0.9220   | –              |
|                            | STARE    | 0.779       | 0.9409      | 0.9240   | –              |
| Anzalone et al. [76]       | DRIVE    | –           | –           | 0.9419   | –              |
| Farnell et al. [77]        | STARE    | –           | –           | –        | 0.940          |
|                            | ARIA     | –           | –           | –        | 0.895          |
| Vlachos and Dermatas [78]  | DRIVE    | 0.747       | 0.955       | 0.929    | –              |

highest accuracy when applied to a range of retinal images from the DRIVE and STARE datasets.

### 3.6. Model based approaches

These approaches apply the explicit vessel models to extract the retinal vessels. We classify the model based approaches into two categories; (1) vessel profile models and (2) deformable models.

#### 3.6.1. Vessel profile models

The vessel cross-sectional intensity profiles approximate a Gaussian shape, or a mixture of Gaussians in case of central vessel reflex. Other profiles like the second-order derivative Gaussian, the cubic spline, or Hermite polynomial profile can be readily substituted. The more complex scenario is to include the non-vessel features like bright or dark lesions and the background characteristic in the vessel detection model to increase the segmentation accuracy in difficult imaging conditions. The flat background has also been assumed in some profile models for the vessel section. Vessel crossing and branching can further complicate the profile model.

Vermeer et al. [79] modeled the vessel profile as Laplacian to incorporate the central vessel reflex. The image is convolved with a 2-D Laplace kernel and the aligned vessel fragments in the MFR image are connected followed by the removal of smaller objects. The inner parts of the vessel are identified by morphological closing to produce candidate objects. The algorithm accuracy is affected by parameter selection if used with different retinal datasets. The algorithm is analyzed on GDx generated images and yields a TPR of 0.924, a FPR of 0.079, and sensitivity of 92.4% and specificity of 92.1%.

Mahadevan et al. [80] presents a set of algorithms for a robust and modular framework for vessel detection in noisy images. The authors presented the estimation of the log likelihood of vessel parameters in a noisy environment using three models; the Huber's censored likelihood ratio test [106], the ranked ordered test [107] for log likelihood and the robust model selection [108] based on nonlinear least squares fitting. The framework is adaptable to incorporate a variety of vessel profile models including Gaussian, derivatives of Gaussian and dual Gaussian and various noise models like Gaussian noise and Poisson noise. The framework is tested on a synthetic phantom as well as sequences of clinical images and

the results are compared with that of the matched filter [46] and the direct exploratory vessel tracing algorithm [67] and report an improvement of 43.7% and 145.7%, respectively. An extension [109] of this vessel detection framework is also proposed by the authors with the inclusion of a generalized dual-Gaussian cross-sectional profile for improved detection of vessels containing a central vessel reflex.

A multi-resolution Hermite model is proposed for vascular segmentation by Li et al. [81], which employs a two-dimensional Hermite function intensity model in a quad-tree structure over a range of spatial resolutions. The vessel modeling and estimation technique is based on a Hermite polynomial instead of a mixture Gaussian [84,102] to incorporate the central light reflex. Vessel segments with their local directions, widths and amplitudes, and bifurcations are identified explicitly by a local model which also incorporates the estimation for a piecewise linear background variation. A block based multiresolution approach is used in combination with an expectation-maximization (EM) optimization scheme to fit the local model parameters. The local models of vessel segments and bifurcations are linked using a stochastic Bayesian approach to infer the global vascular structure. The methodology achieves a sensitivity and specificity of 0.752 and 0.980 on STARE and 0.780 and 0.978 on the DRIVE database.

Lam and Hong [82] proposed a novel vessel segmentation algorithm for pathological retinal images based on the divergence of vector fields. In this method the centerlines are detected using the normalized gradient vector field, and then the blood vessel-like objects are detected using the gradient vector field of a pixel. The spurious detected blood vessel-like objects are pruned according to the distance from detected centerlines. All the pathological retinal images in the STARE database are used to evaluate the proposed method and an average accuracy of 0.9474 and area under the ROC curve of 0.9392 is reported.

The algorithm presented by Lam et al. [83] is based on regularization based multiconcavity modeling and is able to handle both normal and pathological retinas with bright and dark lesions simultaneously. Three different concavity measures are proposed to detect blood vessels and each of these measures is designed to address the negative impact produced by the lesions for identifying the normal vessels. The steep intensity transition pattern of bright lesions is distinguished from vessels with differential concavity measures.

A line shape concavity measure is used to distinguish the irregular shape intensity structure of dark lesions from the line shape intensity structure of the blood vessel. A locally normalized concavity measure is used to filter out the noise. Finally, the features obtained from these concavity measures are combined according to their statistical and geometrical properties and later a lifting technique is used for optimizing the regularized solution towards the ideal vessel shape. The effectiveness and robustness of the proposed method are evaluated on DRIVE and STARE resulting in an average accuracy of 0.9472 and 0.9567 and the area under the ROC curve as 0.9614 and 0.9739 for DRIVE and STARE, respectively.

The structural and functional features of dual-wavelength retinal fundus images recorded at 570 and 600 nm [84] are exploited for vessel segmentation and identification as arteries and veins. In this algorithm, the dual-Gaussian model initially used by Gao et al. [102] is extended to estimate the cross sectional intensity profile of retinal vessels.

A universal representation of vessel cross-sectional profiles in the Fourier domain, utilizing phase congruency to characterize this representation is proposed by Zhu [85]. The proposed Fourier profile accommodates for upward and downward cross-sectional profiles with varying sharpness, and takes into account the vessel inner part. An input image is transformed by 24 log-Gabor filters covering six directions and four scales in symmetric and anti-symmetric pairs. The symmetry and asymmetry of local Fourier components is measured using the scale-invariant property and the Kovesei phase congruency model [110]. The singular value decomposition (SVD) on the 24 asymmetric values of each pixel location is performed resulting in maximum ( $\alpha$ ) and the minimum ( $\beta$ ) eigenvalues. A point feature location is identified by large magnitude of  $\alpha$ . Non linear point features (bifurcation and crossovers) are characterized by large and similar values of  $\alpha$  and  $\beta$ . The non-linear features belonging to non vessel structures are excluded. The asymmetric and symmetric images are binaries to produce an initial region and a set of boundary points separating the vessel from background, respectively, which are further utilized in a region growing process for vessel detection.

### 3.6.2. Deformable models

The methodologies based on deformable models for vessel segmentation can be further divided into two categories; (1) parametric deformable models and (2) geometric deformable models.

**3.6.2.1. Parametric models.** *Active contour models*, informally known as *snakes*, [111] are the curves defined within an image domain that can move under the influence of internal forces within the curve itself and external forces derived from the image data. The internal and external forces are defined so that the snake will conform to an object boundary or other desired features within an image. The *internal (smoothing) forces* produce *tension* and *stiffness* that constrain the behavior of the snake and the *external forces* may be specified by a supervising process or a human user. Some of the advantages of snakes over classical feature attraction techniques are that they are autonomous and self-adapting in their search for a minimal energy state. They can also be easily manipulated using

external image forces. They can be used to track dynamic objects in temporal as well as the spatial dimensions. The main limitation of the models are that they usually only incorporate edge information, ignoring other image characteristics) possibly combined with some prior expectation of shape. Due to this they often overlook minute features in the process of minimizing the energy over the entire path of their contours. They are required to be initialized close to the feature of interest if they are to avoid being trapped by other local minima. Their accuracy is governed by the convergence criteria used in the energy minimization technique; higher accuracies require tighter convergence criteria and hence, longer computation times. Snakes are often used in applications like object tracking, shape recognition, segmentation, edge detection and stereo matching. A number of authors have investigated the use of active contour models in retinal vascular segmentation.

Espona et al. [86] use the classical snake in combination with blood vessel topological properties to extract the vasculature from retinal image. The snake is guided by a vessel crease which is actually the approximation of vessel centerlines extracted using Multilevel Set Extrinsic Curvature based on the Structure Tensor. The snake is initialized and deformed based on the external energy defined by the vessel crease. The nodes located in the vessel crease make the snake evolve along the vessel center line by energy minimization to locate the vessel edges. First, the creases and edge images and energy maps are calculated on the original image. Next, a circumference surrounding the optic nerve is traced and then the intersections of creases and this circumference are obtained. A snake is initialized with the intersection of vessel creases and the optic disk circumference and is evolved iteratively minimizing the local energy function keeping in view the discontinuity in vascular structure. The accuracy, sensitivity and specificity of the algorithm is reported to be 0.9316, 0.6634 and 0.9682, respectively on DRIVE. The authors proposed [87] an improvement in the algorithms by introducing morphological operations for vessel crease extraction and the fine tuning of snake energy minimizing parameters. The improved accuracy, sensitivity and specificity are 0.9352 0.7436 and 0.9615, respectively on DRIVE.

Al-Diri and Hunter introduce Ribbon of Twin [112], a parametric active contour model, which uses two contours coupled by spring models to overcome initialization and localized feature problems; and the “ribbon” method, which couples two snakes with a consistent width parameter. The model uses four contours to extract segments of vessel boundaries, a ribbon joining two twins. In this model, two twins of contours represent a ribbon along a vessel, with one twin on each edge of the vessel. Each twin consists of two contours, one inside and one outside the vessel. Each contour consists of a number of nodes. Corresponding nodes on the four contours are connected together to form a single integrated model. The two outside contours are connected by pull forces to the inside contours, while the inside contours are connected by push forces with each other. The model converges when the maximum distance between both contours inside the twin are less than a certain threshold. The edges of the vessel are captured from both sides by inside and outside contours. The distance between the inside contours give the measure of vessel width. The model exhibits robust behavior on retinal

images with noise and those that have closely parallel vessels, blurred vessel edges, central vessel reflex and very fine vessels.

An algorithm for the extraction of segment profiles of blood vessels which integrates vessel segmentation and width measurement based on the Ribbon of Twin active contour model is presented by Al-Diri et al. [88]. Initially, the tramline filter is used to locate an initial set of potential vessel segment centerline pixels. Then the segment growing algorithm converts the tramline pixel map into a set of segments, each consisting of a series of profiles, while discarding false positive pixels. The growing algorithm uses the ROT active contour model, i.e. two pairs of contours to capture each vessel edge, while maintaining width consistency. Later, the junction resolution algorithm extends the discrete segments and resolves various crossings, junctions and joinings. The algorithm accurately locates the vessel edges under challenging conditions, including noisy blurred edges, closely parallel vessels, light reflex phenomena, and very fine vessels. The algorithm achieves the values of 72.82 and 95.51 for sensitivity and specificity, respectively for DRIVE and 75.21 and 96.81 sensitivity and specificity, respectively on STARE. The junction resolution algorithm is evaluated on the first five images of DRIVE for detection of bifurcations, bridges and leaves, and resulted in precision rates of 89%, 95%, and 90%, respectively. The width measurement is reported on the REVIEW database [25].

**3.6.2.2. Geometric models.** The geometric models for active contours are based on the theory of curve evolution geometric flows. These models are usually implemented using the level-set based numerical algorithm. The level set method (LSM) is a numerical technique for tracking interfaces and shapes. The advantage of the level set method is that numerical computations involving curves and surfaces can be performed on a fixed Cartesian grid without having to parameterize these objects.

Sum and Cheung [89] proposed a modification in the Chan and Vese [113] model by incorporating the local image contrast into a level-set-based active contour to handle non-uniform illumination. The approach is evaluated with experiments involving both synthetic images and clinical angiograms.

A methodology based on nonlinear projections is proposed by [90]. The nonlinear projection can be used to capture the texture structures in images. The green channel image is projected onto a closed convex set consisting of the oscillating functions with zero mean. The oscillating components of scanning retinal images are adopted to capture the features of blood vessel networks. The segmented vessel tree is obtained by an adaptive thresholding method based on the variational image binarization algorithm [114]. Morphological post processing is also applied to the resulting binary image. The algorithm reports the TPR, FPR and accuracy for DRIVE (0.754%, 0.0228% and 96.1%) and for STARE (0.9373%, 0.0264% and 90.87%) respectively.

The performance of model based approaches for retinal vessel segmentation is summarized in Table 8, where the highest accuracy is reported for Lam [66], an algorithm based on the divergence of vector fields, on the DRIVE and STARE datasets.

### 3.7. Parallel hardware based implementations

The high computational cost of retinal vessel segmentation algorithms and requirements for real-time performance is addressed by parallel hardware based implementation of algorithms. One attractive paradigm for parallel real-time image processing is represented by cellular neural networks [115,116], which can be implemented on VLSI chips. The insight segmentation and registration Toolkit [105] is also used for parallel implementation for vessel segmentation algorithms in high resolution images. The toolkit provides leading-edge segmentation and registration algorithms in two, three, and more dimensions and is implemented in C++ and it is wrapped for Tcl, Python and Java.

Alonso-Montes et al. [91] presented a hardware based algorithm where the segmentation is obtained through CNN-based histogram equalisation and modification, local adaptive thresholding, and morphological opening. The Pixel level snakes (PLS) [117], a topographic iterative active contour technique, is used to extract the vascular tree using the initial contour of vessels and their external potential image. The algorithm is simulated in the MATCNN [118] environment using  $3 \times 3$  linear CNN templates and implemented on a CNN chip-set architecture based on the CNN Universal Machine (CNUM) [116] paradigm.

A pixel-parallel approach for fast retinal vessel extraction is presented [92] which in fact redefines the original proposal [91] in terms of local dynamic convolutions and morphological operations together with arithmetic and logical operations to be implemented and tested in a fine-grain single instruction multiple data (SIMD) parallel processor array [119]. The exterior of vessels are found by parallel active contour, the pixel-level snakes [120]. The algorithm reported an average accuracy of 0.9180 and a processing time of 0.19 s per image on the DRIVE database.

The above mentioned methods rely on several design parameters: the scaling factors of local mean and variance, the neighborhood size, and the structuring element for morphological operations. Since no guidelines are available for their settings, they must be empirically tuned. Moreover, nonlinear CNN templates are required for local estimation of the variance in the image. To overcome these issues, Renzo et al. [121,122] exploited the geometrical properties of blood vessels by calculating the line strength measures [34,123] for the blood vessels in the green plane of the colored retinal image. The line strength image could be realized with simple CNN templates in a multistep operation with virtual template expansion. The proposed CNN algorithm requires only linear space-invariant  $3 \times 3$  templates, so it could be implemented using one of the existing CNN chips. For example, the ACE16K chip is a  $128 \times 128$  array with 7-bit accuracy, eight analog greyscale memories per cell, and 32 stored templates [124]. The algorithm gives better area under ROC and accuracy values for the same neighborhood size as compared with [92].

A parallel implementation [93] of multi-scale vessel segmentation [73] algorithm based on ITK is capable of achieving accuracy comparable to its serial counterpart while providing processing 8–10 times faster which is advantageous for handling for higher resolution images and larger datasets. The image is divided into sub-images having overlapping

**Table 8 – Performance measures for the model based methodologies.**

| Methodology         | Database | Sensitivity | Specificity | Accuracy | Area under ROC |
|---------------------|----------|-------------|-------------|----------|----------------|
| Human observer      | DRIVE    | 0.776330    | 0.972314    | 0.947046 | –              |
|                     | STARE    | 0.895177    | 0.938422    | 0.934891 | –              |
| Vermeer et al. [79] | GDx      | 0.924       | 0.921       | –        | –              |
|                     | STARE    | –           | –           | 0.9287   | 0.9187         |
| Li et al. [81]      | DRIVE    | 0.780       | 0.978       | –        | –              |
|                     | STARE    | 0.752       | 0.980       | –        | –              |
| Lam and Hong [82]   | STARE    | –           | –           | 0.9474   | 0.9392         |
| Lam et al. [83]     | DRIVE    | –           | –           | 0.9472   | 0.9614         |
|                     | STARE    | –           | –           | 0.9567   | 0.9739         |
| Espona et al. [86]  | DRIVE    | 0.6634      | 0.9682      | 0.9316   | –              |
| Espona et al. [87]  | DRIVE    | 0.7436      | 0.9615      | 0.9352   | –              |
| Al-Diri et al. [88] | DRIVE    | 0.7282      | 0.9551      | –        | –              |
|                     | STARE    | 0.7521      | 0.9681      | –        | –              |
| Zhang et al. [90]   | DRIVE    | –           | 0.9772      | 0.9610   | –              |
|                     | STARE    | 0.7373      | 0.9736      | 0.9087   | –              |

regions and distributed across computers for feature extraction and region growing and later the segmentation results are combined. The implementation achieves 0.644, 0.033 and 0.925 TPR, FPR and accuracy, respectively on DRIVE and 0.769, 0.0551 and 0.926 TPR, FPR and accuracy, respectively on STARE. Table 9 illustrated the performance metrics for the algorithms based on parallel hardware implementations.

#### 4. Discussion

The performance of algorithms based on supervised classification is better in general than their counterparts. Almost all the supervised methods report the area under ROC of approximately 0.95 and among them Soares et al. [33] reported the highest. However, these methods do not work very well on the images with non uniform illumination as they produce false detection in some images on the border of the optic disc, hemorrhages and other types of pathologies that present strong contrast. Matched filtering has been extensively used for automated retinal vessel segmentation. Many improvements and modifications are proposed since the introduction of the Gaussian matched filter by Chaudhuri et al. [46]. The parametric optimization of the matched filter using exhaustive search [50] and ant optimization [53] resulted in an improvement of segmentation accuracy from 0.8773 to 0.9535. The concept of steerable filters [47] helps in the reduction of processing time. The matched filtering alone cannot handle

vessel segmentation in pathological retinal images; therefore it is often employed in combination with other image processing techniques [53,75]. The problem of the central vessel reflex is solved by employing the mixture of the Gaussian model [84,109] and Ribbon of Twin Active Contour [88]. The confidence measures and edge measures defined by Sofka and Stewart [75] deals with the problem of overlapping of the non-vessel structures like the retinal boundary and the optic disk in vasculature extraction. The use of multi concavity modeling [83] and the divergence of vector fields [82] is quite successful in dealing with pathologies in the form of cotton wool spots, bright and dark lesions and exudates. The background homogenization followed by the use of gray level and moment-invariant based features for supervised classification [39] is observed to be training set robust. The classifier is trained on the DRIVE database and the application to the STARE database yields high accuracy. The combination of radial projections with steerable wavelets and semi-supervised classification [38] resulted in very good performance in the detection of narrow and low contrast vessels, thus producing highest sensitivity.

The Gabor Wavelets are very useful in retinal image analysis. Besides vessel segmentation [33], [35] and optic disk detection [125], the Gabor wavelet transform has also been utilized for the robust fractal analysis of the retinal vasculature [126].

It is observed that some papers describe the performance in terms of accuracy and area under ROC whereas the other

**Table 9 – Performance measures for parallel hardware implementation based methods.**

| Methodology                | Database | Sensitivity | Specificity | Accuracy | Area under ROC |
|----------------------------|----------|-------------|-------------|----------|----------------|
| Human observer             | DRIVE    | 0.7763      | 0.9723      | 0.9470   | –              |
|                            | STARE    | 0.8951      | 0.9384      | 0.9348   | –              |
| Renzo et al. [121]         | DRIVE    | –           | –           | 0.9348   | 0.9261         |
| Alonso-Montes [92]         | DRIVE    | –           | –           | 0.9185   | 0.9011         |
| Palomera-Perez et al. [93] | DRIVE    | 0.64        | 0.967       | 0.9250   | –              |
|                            | STARE    | 0.769       | 0.9449      | 0.926    | –              |

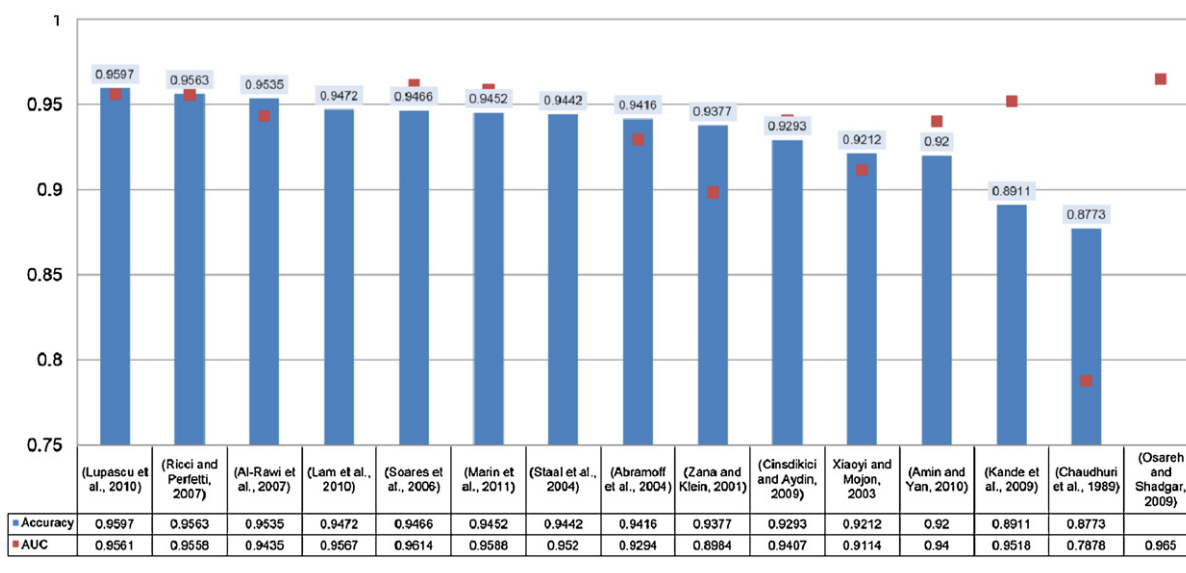


Fig. 6 – Accuracy and area under curve for DRIVE.

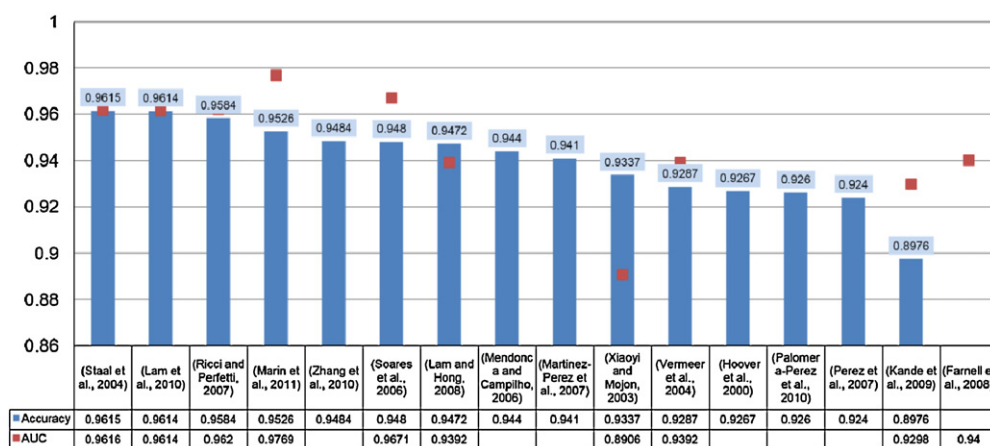


Fig. 7 – Accuracy and area under curve for STARE.

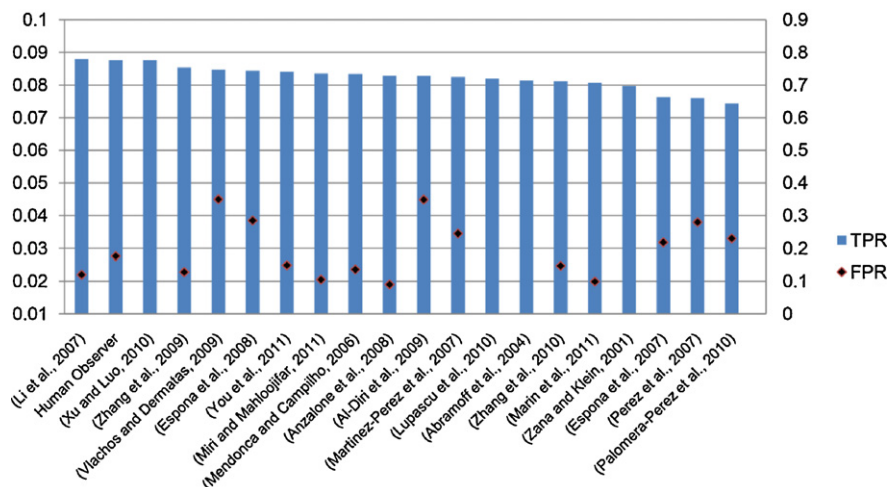


Fig. 8 – TPR and FPR for DRIVE database.

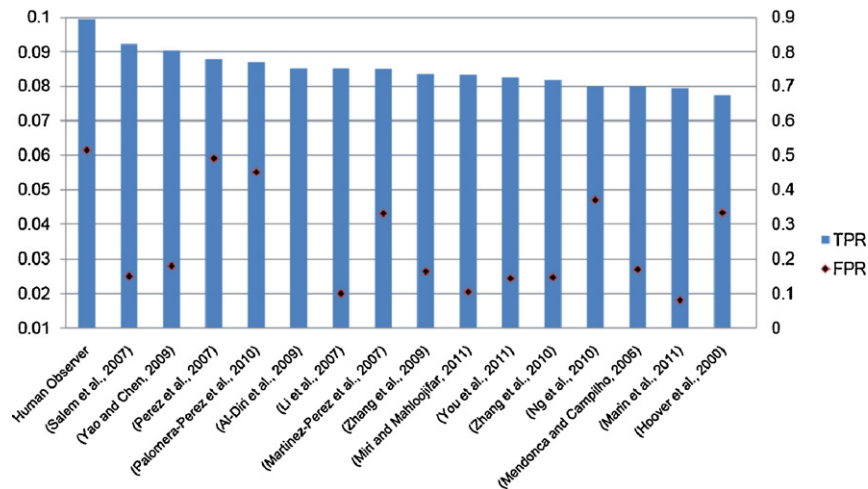


Fig. 9 – TPR and FPR for STARE database.

articles choose TPR and FPR (Sensitivity and 1-Specificity, respectively) for reporting the performance. The plots for the accuracy and area under the ROC curve for some of the reviewed segmentation methodologies are illustrated in Figs. 6 and 7 for the DRIVE and STARE databases, respectively. The sensitivity (TPR) and specificity (1-FPR) plots of some of the reviewed retinal vessel segmentation algorithms are shown in Fig. 8 (for DRIVE) and Fig. 9 (for STARE).

## 5. Conclusion

The segmentation of the blood vessels in the retina has been a heavily researched area in recent years. The accurate extraction of the retinal vascular tree forms the backbone of many automated computer aided systems for screening and diagnosis of cardiovascular and ophthalmologic diseases. Even though many promising techniques and algorithms have been developed, there is still room for improvement in blood vessel segmentation methodologies. Only few of the reviewed algorithms serve for pathological and noisy retinal images [80,82,83,85,89] and those that are suitable for analysis of images where vessels contain a central reflex are even less [34,39,88], as illustrated in Table 2. Most of the techniques available in the literature are evaluated on a limited range of datasets which include twenty images each from the DRIVE and STARE databases. The performance measures presented in most of the papers are calculated on a small number of images of particular morphological characteristics. The limited range of images in the DRIVE and STARE databases do not cater for the image related characteristics such as, inter-image and intra image variability in luminance, drift in contrast and uneven background gray level values. The development of techniques which work for images acquired from different imaging equipment, under different environmental conditions is also an open area for research in vessel segmentation algorithms.

One of the real-life practical applications of automatic blood vessel segmentation in health care includes diabetic screening programs. The development of research software

applications which integrate various computer-assisted retinal image analysis algorithms such as vessel extraction, registration, landmark tracing for pathologies, vessel caliber measurement and branching and crossover detection is new research direction. These kinds of applications can facilitate progress in studying the correlations of ocular fundus anatomy with retinal diseases. There is a requirement of solution for screening programs where the evaluation of large image datasets and the collaboration between the experts and healthcare centers is needed. SIRIUS [127] (System for the Integration of Retinal Images Understanding Services) is a web-based system for retinal image analysis which provides a collaborative framework for experts. Sirius consists of a web based client user interface, a web application server for service delivery and the service module for image processing tasks. The system allows the sharing of images and processed results between remote computers and provides automated methods to diminish inter-expert variability in the analysis of the images. A service module for the analysis of retinal microcirculation using a semi-automatic methodology for the computation of the arteriolar-to-venular ratio (AVR) is included in the framework. The service module could be further extended to include vessel width and tortuosity measures and detection of other pathologies in retinal images. Retinopathy Online Challenge (ROC) [26], a multiyear online competition for various aspects of diabetic retinopathy detection is also an excellent collaborative effort for improving the computer aided detection and diagnosis of diabetic retinopathy. The RIVERS (Retinal Image Vessel Extraction and Registration System) project [128] [129] can also be considered as an initiative in this direction. VAMPIRE [130] (Vascular Assessment and Measurement Platform for Images of the REtina) is a software application for semi-automatic quantification of retinal vessel properties. The system aims to provide efficient and reliable detection of retinal landmarks (optic disc, retinal zones, main vasculature), and quantify key parameters used frequently in investigative studies which includes vessel width, vessel branching coefficients and tortuosity measures. The creation of ground truths for vessel segmentation is a crucial task which entails training and skill. Live-Vessel [68] is a

semi-automatic and interactive medical image segmentation software tool for locating vessels and vascular trees in 2D color medical images.

Vessel extraction is often the first stage of processing before pathology detection algorithms are applied. There are thousands of images acquired from various types of fundus camera. In addition, most of the published algorithms are evaluated on the limited image datasets of DRIVE and STARE. The resolutions of images from the STARE and DRIVE datasets are limited to 0.4 and 0.3 megapixels, respectively. While this lower resolution is acceptable for certain analyses like fractal dimension or tortuosity, calculating the vessel diameter normally requires higher resolution images to achieve higher precision. Mosher [131] has compared central retinal artery equivalents (CRAE) and central retinal vein equivalents (CRVE) of vessels measured from images of 6.3 megapixel resolution captured with a digital camera and digitized images taken with a film camera. Some artifacts like the nerve fiber are more visible in the higher resolution images and may result in higher false positives. The classification of retinal blood vessels into arterioles and venules is essential in clinical diagnosis for vessel caliber measurement and to calculate the CRAE/CRVE/AVR. Therefore, in order to expand the utility of vessel segmentation algorithms for healthcare, there is a need to create larger datasets with available ground truths which include the labeling of vessels, other anatomical structures and classification of arterioles and venules. Besides DRIVE and STARE, the other publicly available retinal image databases include REVIEW [25] for vessel width measures, MESSIDOR [24], ImageRet [23] and ARIA Online [22] for diabetic retinopathy, ROC microaneurysm set [26] for microaneurysm detection and the VICAVER database [27] used for the computation of the A/V Ratio.

Advances in ophthalmic imaging systems make it possible to gather high volumes of patient images for screening. Processing of these images in computer aided diagnostic systems requires fast segmentation algorithms robust enough to process the images acquired from various image capture systems and imaging conditions. The algorithms exploiting parallel and hardware based implementations [91,93,121] offer a solution providing high computation speed that is required in real-time applications.

Most of the segmentation methodologies are evaluated on the retinal images of adults. The morphological characteristics of retinal images of premature infants, babies and children are very different than that of the adult retina. Choroidal vessels are more visible alongside the retinal vessels in retinal images taken from premature infants [132]. A bright central reflex on the vessels and illumination artifacts contribute to challenges in image processing when retinal images from school children are considered [133]. Three-dimensional optical coherence tomography (3D OCT) imaging is used to obtain detailed images from within the retina and therefore improves visualization and mapping of the retinal microstructure. The availability of ultra-wide field retinal images [134] provided by Optos technologies [134] and 3D OCT triggers the need to develop faster, more accurate 3D segmentation techniques, particularly focusing on retinal images taken from an ultra wide field of view, with pathologies and backgrounds of

uneven intensity and illumination distribution. Perez-Rovira et al. [135] present a nice improvement in this direction.

Accuracy and robustness of the segmentation process is essential to achieve a more precise and efficient computer aided diagnostic system. It is not expected that the vessel segmentation systems will replace the experts in diagnosis; rather they will reduce the workload of the experts in processing the sheer volume of medical images. This paper provides a survey of current retinal blood vessel segmentation methods. We have covered both early and recent literature focusing on retinal vessel segmentation algorithms and techniques. Our aim was to introduce the current segmentation techniques, give the reader a framework for the existing research and to introduce the array of retinal vessel segmentation algorithms found in literature. The current trends, the future directions and the open problems in automated blood vessel segmentation are also discussed. We will continue to update this review with new references and will post it on <http://sec.kingston.ac.uk/retinal>.

---

## Conflicts of interest

There are no conflicts of interest.

## REFERENCES

- 
- [1] J.J. Kanski, *Clinical Ophthalmology*, 6th ed., Elsevier Health Sciences, London, UK, 2007.
  - [2] T. Teng, M. Lefley, D. Claremont, Progress towards automated diabetic ocular screening: a review of image analysis and intelligent systems for diabetic retinopathy, *Medical and Biological Engineering and Computing* 40 (2002) 2–13.
  - [3] C. Heneghan, J. Flynn, M. O’Keefe, M. Cahill, Characterization of changes in blood vessel width and tortuosity in retinopathy of prematurity using image analysis, *Medical Image Analysis* 6 (2002) 407–429.
  - [4] A. Haddouche, M. Adel, M. Rasigni, J. Conrath, S. Bourennane, Detection of the foveal avascular zone on retinal angiograms using Markov random fields, *Digital Signal Processing* 20 (2010) 149–154.
  - [5] E. Grisan, A. Ruggeri, A divide et impera strategy for automatic classification of retinal vessels into arteries and veins, in: *Engineering in Medicine and Biology Society, 2003. Proceedings of the 25th Annual International Conference of the IEEE*, vol. 891, 2003, pp. 890–893.
  - [6] M. Foracchia, Extraction and quantitative description of vessel features in hypertensive retinopathy fundus images, in: E. Grisan (Ed.), *Book Abstracts 2nd International Workshop on Computer Assisted Fundus Image Analysis*, 2001, p. 6.
  - [7] J. Lowell, A. Hunter, D. Steel, A. Basu, R. Ryder, R.L. Kennedy, Measurement of retinal vessel widths from fundus images based on 2-D modeling, *IEEE Transactions on Medical Imaging* 23 (2004) 1196–1204.
  - [8] F. Zana, J.C. Klein, A multimodal registration algorithm of eye fundus images using vessels detection and Hough transform, *IEEE Transactions on Medical Imaging* 18 (1999) 419–428.
  - [9] K. Fritzsche, A. Can, H. Shen, C. Tsai, J. Turner, H.L. Tanenbaum, C.V. Stewart, B. Roysam, J.S. Suri, S. Laxminarayan, Automated model based segmentation, tracing and analysis of retinal vasculature from digital

- fundus images, in: *State-of-The-Art Angiography, Applications and Plaque Imaging Using MR, CT Ultrasound and X-rays*, Academic Press, 2003, pp. 225–298.
- [10] L. Huiqi, O. Chutatape, Automated feature extraction in color retinal images by a model based approach, *IEEE Transactions on Biomedical Engineering* 51 (2004) 246–254.
- [11] C. Mariño, G. Penedo, M. Penas, J. Carreira, F. Gonzalez, Personal authentication using digital retinal images, *Pattern Analysis and Applications* 9 (2006) 21–33.
- [12] C. Köse, C. Ikibas, A personal identification system using retinal vasculature in retinal fundus images, *Expert Systems with Applications* 38 (2011) 13670–13681.
- [13] P. Felkel, R. Wegenkittl, A. Kanitsar, Vessel tracking in peripheral CTA datasets – an overview, in: *Computer Graphics, Spring Conference on, 2001, 2001*, pp. 232–239.
- [14] K. Buhler, P. Felkel, A.L. Cruz, Geometric methods for vessel visualization and quantification – a survey, *Geometric Modelling for Scientific Visualization* (2003) 399–421.
- [15] C. Kirbas, F. Quek, A review of vessel extraction techniques and algorithms, *ACM Computing Surveys* 36 (2004) 81–121.
- [16] M.S. Mabrouk, N.H. Solouma, Y.M. Kadah, Survey of retinal image segmentation and registration, *ICGST International Journal on Graphics, Vision and Image Processing* 6 (2006) 1–11.
- [17] R.J. Winder, P.J. Morrow, I.N. McRitchie, J.R. Bailie, P.M. Hart, Algorithms for digital image processing in diabetic retinopathy, *Computerized Medical Imaging and Graphics* 33 (2009) 608–622.
- [18] O.R.A.U. Faust, E. Ng, K.-H. Ng, J. Suri, Algorithms for the automated detection of diabetic retinopathy using digital fundus images: a review, *Journal of Medical Systems* 36 (2010) 1–13.
- [19] B. Cassin, S.A.B. Solomon, *Dictionary of Eye Terminology*, 2nd ed., Triad Publishing Company, 1990.
- [20] M. Niemeijer, J.J. Staal, B.v. Ginneken, M. Loog, M.D. Abramoff, DRIVE: digital retinal images for vessel extraction, <http://www.isi.uu.nl/Research/Databases/DRIVE>, 2004.
- [21] A.D. Hoover, V. Kouznetsova, M. Goldbaum, Locating blood vessels in retinal images by piecewise threshold probing of a matched filter response, *IEEE Transactions on Medical Imaging* 19 (2000) 203–210.
- [22] ARIA Online, Retinal Image Archive [http://www.eyeharmony.com/aria\\_online/](http://www.eyeharmony.com/aria_online/), 2006.
- [23] T. Kauppi, V. Kalesnykiene, J.-K. Kamarainen, L. Lensu, I. Sorri, A. Raninen, R. Voutilainen, J. Pietilä, H. Kälviäinen, H. Uusitalo, DIARETDB1 diabetic retinopathy database and evaluation protocol, in: *Medical Image Understanding and Analysis (MIUA2007)*, Aberystwyth, Wales, UK, 2007, pp. 61–65.
- [24] MESSIDOR: Methods for Evaluating Segmentation and Indexing techniques Dedicated to Retinal Ophthalmology, <http://messidor.crihan.fr/index-en.php>, 2004.
- [25] B. Al-Diri, A. Hunter, D. Steel, M. Habib, T. Hudaib, S. Berry, REVIEW – a reference data set for retinal vessel profiles, in: *Engineering in Medicine and Biology Society, 2008 EMBS 2008. 30th Annual International Conference of the IEEE*, 2008, pp. 2262–2265.
- [26] M. Niemeijer, B. van Ginneken, M.J. Cree, A. Mizutani, G. Quellec, C.I. Sanchez, B. Zhang, R. Hornero, M. Lamard, C. Muramatsu, X. Wu, G. Cazuguel, J. You, A. Mayo, L. Qin, Y. Hatanaka, B. Cochener, C. Roux, F. Karray, M. Garcia, H. Fujita, M.D. Abramoff, Retinopathy online challenge: automatic detection of microaneurysms in digital color fundus photographs, *IEEE Transactions on Medical Imaging* 29 (2009) 185–195.
- [27] The VICAVR database, <http://www.varpa.es/vicavr.html>, 2010.
- [28] K. Akita, H. Kuga, A computer method of understanding ocular fundus images, *Pattern Recognition* 15 (1982) 431–443.
- [29] R. Nekovei, S. Ying, Back-propagation network and its configuration for blood vessel detection in angiograms, *IEEE Transactions on Neural Networks* 6 (1995) 64–72.
- [30] C. Sinthanayothin, J.F. Boyce, H.L. Cook, T.H. Williamson, Automated localisation of the optic disc, fovea, and retinal blood vessels from digital colour fundus images, *British Journal of Ophthalmology* 83 (1999) 902–910.
- [31] M. Niemeijer, J.J. Staal, B. van Ginneken, M. Loog, M.D. Abramoff, Comparative study of retinal vessel segmentation methods on a new publicly available database, in: J.M. Fitzpatrick, M. Sonka (Eds.), *SPIE Medical Imaging*, SPIE, 2004, pp. 648–656.
- [32] J. Staal, M.D. Abramoff, M. Niemeijer, M.A. Viergever, B. van Ginneken, Ridge-based vessel segmentation in color images of the retina, *IEEE Transactions on Medical Imaging* 23 (2004) 501–509.
- [33] J.V.B. Soares, J.J.G. Leandro, R.M. Cesar, H.F. Jelinek, M.J. Cree, Retinal vessel segmentation using the 2-D Gabor wavelet and supervised classification, *IEEE Transactions on Medical Imaging* 25 (2006) 1214–1222.
- [34] E. Ricci, R. Perfetti, Retinal blood vessel segmentation using line operators and support vector classification, *IEEE Transactions on Medical Imaging* 26 (2007) 1357–1365.
- [35] A. Osareh, B. Shadgar, Automatic blood vessel segmentation in color images of retina, *Iranian Journal Of Science And Technology Transaction B – Engineering* 33 (2009) 191–206.
- [36] L. Xu, S. Luo, A novel method for blood vessel detection from retinal images, *BioMedical Engineering Online* 9 (2010) 14.
- [37] C.A. Lupascu, D. Tegolo, E. Trucco, FABC: retinal vessel segmentation using AdaBoost, *IEEE Transactions on Information Technology in Biomedicine* 14 (2010) 1267–1274.
- [38] X. You, Q. Peng, Y. Yuan, Y.-m. Cheung, J. Lei, Segmentation of retinal blood vessels using the radial projection and semi-supervised approach, *Pattern Recognition* 44 (2011) 2314–2324.
- [39] D. Marin, A. Aquino, M.E. Gegundez-Arias, J.M. Bravo, A new supervised method for blood vessel segmentation in retinal images by using gray-level and moment invariants-based features, *IEEE Transactions on Medical Imaging* 30 (2011) 146–158.
- [40] Y.A. Tolias, S.M. Panas, A fuzzy vessel tracking algorithm for retinal images based on fuzzy clustering, *IEEE Transactions on Medical Imaging* 17 (1998) 263–273.
- [41] J. Ng, S.T. Clay, S.A. Barman, A.R. Fielder, M.J. Moseley, K.H. Parker, C. Paterson, Maximum likelihood estimation of vessel parameters from scale space analysis, *Image and Vision Computing* 28 (2010) 55–63.
- [42] A. Simó, E. de Ves, Segmentation of macular fluorescein angiographies. A statistical approach, *Pattern Recognition* 34 (2001) 795–809.
- [43] G.B. Kande, P.V. Subbaiah, T.S. Savithri, Unsupervised fuzzy based vessel segmentation in pathological digital fundus images, *Journal of Medical Systems* 34 (2009) 849–858.
- [44] S. Salem, N. Salem, A. Nandi, Segmentation of retinal blood vessels using a novel clustering algorithm (RACAL) with a partial supervision strategy, *Medical and Biological Engineering and Computing* 45 (2007) 261–273.
- [45] F. Villalobos-Castaldi, E. Felipe-Riverón, L. Sánchez-Fernández, A fast, efficient and automated method to extract vessels from fundus images, *Journal of Visualization* 13 (2010) 263–270.

- [46] S. Chaudhuri, S. Chatterjee, N. Katz, M. Nelson, M. Goldbaum, Detection of blood vessels in retinal images using two-dimensional matched filters, *IEEE Transactions on Medical Imaging* 8 (1989) 263–269.
- [47] B. Kochner, D. Schuhmann, M. Michaelis, G. Mann, K.-H. Englmeier, Course tracking and contour extraction of retinal vessels from color fundus photographs: most efficient use of steerable filters for model-based image analysis, in: *Medical Imaging 1998: Image Processing*, SPIE, San Diego, CA, USA, 1998, pp. 755–761.
- [48] L. Gang, O. Chutatape, S.M. Krishnan, Detection and measurement of retinal vessels in fundus images using amplitude modified second-order Gaussian filter, *IEEE Transactions on Biomedical Engineering* 49 (2002) 168–172.
- [49] J. Xiaoyi, D. Mojon, Adaptive local thresholding by verification-based multithreshold probing with application to vessel detection in retinal images, *IEEE Transactions on Pattern Analysis and Machine Intelligence* 25 (2003) 131–137.
- [50] M. Al-Rawi, M. Qutaishat, M. Arrar, An improved matched filter for blood vessel detection of digital retinal images, *Computers in Biology and Medicine* 37 (2007) 262–267.
- [51] L. Sukkaew, B. Uyyanonvara, S.A. Barman, A. Fielder, K. Cocker, Automatic extraction of the structure of the retinal blood vessel network of premature infants, *Journal of the Medical Association of Thailand* 90 (2007) 1780–1792.
- [52] C. Yao, H.-j. Chen, Automated retinal blood vessels segmentation based on simplified PCNN and fast 2D-Otsu algorithm, *Journal of Central South University of Technology* 16 (2009) 640–646.
- [53] M.G. Cinsdikici, D. Aydin, Detection of blood vessels in ophthalmoscope images using MF/ant (matched filter/ant colony) algorithm, *Computer Methods and Programs in Biomedicine* 96 (2009) 85–95.
- [54] B. Zhang, L. Zhang, L. Zhang, F. Karray, Retinal vessel extraction by matched filter with first-order derivative of Gaussian, *Computers in Biology and Medicine* 40 (2010) 438–445.
- [55] M. Amin, H. Yan, High speed detection of retinal blood vessels in fundus image using phase congruency, *Soft Computing – A Fusion of Foundations, Methodologies and Applications* (2010) 1–14.
- [56] F. Zana, J.C. Klein, Segmentation of vessel-like patterns using mathematical morphology and curvature evaluation, *IEEE Transactions on Image Processing* 10 (2001) 1010–1019.
- [57] G. Ayala, T. Leon, V. Zapater, Different averages of a fuzzy set with an application to vessel segmentation, *IEEE Transactions on Fuzzy Systems* 13 (2005) 384–393.
- [58] A.M. Mendonca, A. Campilho, Segmentation of retinal blood vessels by combining the detection of centerlines and morphological reconstruction, *IEEE Transactions on Medical Imaging* 25 (2006) 1200–1213.
- [59] Y. Yang, S. Huang, N. Rao, An automatic hybrid method for retinal blood vessel extraction, *International Journal of Applied Mathematics and Computer Science* 18 (2008) 399–407.
- [60] K. Sun, Z. Chen, S. Jiang, Y. Wang, Morphological multiscale enhancement, fuzzy filter and watershed for vascular tree extraction in angiogram, *Journal of Medical Systems* (2010).
- [61] M.M. Fraz, S.A. Barman, P. Remagnino, A. Hoppe, A. Basit, B. Uyyanonvara, A.R. Rudnicka, C.G. Owen, An approach to localize the retinal blood vessels using bit planes and centerline detection, *Computer Methods and Programs in Biomedicine*, <http://dx.doi.org/10.1016/j.cmpb.2011.08.009>, in press.
- [62] M.S. Miri, A. Mahloojifar, Retinal image analysis using curvelet transform and multistructure elements morphology by reconstruction, *IEEE Transactions on Biomedical Engineering* 58 (2011) 1183–1192.
- [63] I. Liu, Y. Sun, Recursive tracking of vascular networks in angiograms based on the detection-deletion scheme, *IEEE Transactions on Medical Imaging* 12 (1993) 334–341.
- [64] Z. Liang, M.S. Rzeszutarski, L.J. Singerman, J.M. Chokreff, The detection and quantification of retinopathy using digital angiograms, *IEEE Transactions on Medical Imaging* 13 (1994) 619–626.
- [65] O. Chutatape, Z. Liu, S.M. Krishnan, Retinal blood vessel detection and tracking by matched Gaussian and Kalman filters, in: *Engineering in Medicine and Biology Society, 1998. Proceedings of the 20th Annual International Conference of the IEEE*, vol. 3146, 1998, pp. 3144–3149.
- [66] F.K.H. Quek, C. Kirbas, Vessel extraction in medical images by wave-propagation and traceback, *IEEE Transactions on Medical Imaging* 20 (2001) 117–131.
- [67] C. Ali, S. Hong, J.N. Turner, H.L. Tanenbaum, B. Roysam, Rapid automated tracing and feature extraction from retinal fundus images using direct exploratory algorithms, *IEEE Transactions on Information Technology in Biomedicine* 3 (1999) 125–138.
- [68] P. Kelvin, H. Ghassan, A. Rafeef, Live-vessel: extending livewire for simultaneous extraction of optimal medial and boundary paths in vascular images, in: *Proceedings of the 10th International Conference on Medical Image Computing and Computer-Assisted Intervention*, Springer-Verlag, Brisbane, Australia, 2007.
- [69] K.K. Delibasis, A.I. Kechriniotis, C. Tsonos, N. Assimakis, Automatic model-based tracing algorithm for vessel segmentation and diameter estimation, *Computer Methods and Programs in Biomedicine* 100 (2010) 108–122.
- [70] A.F. Frangi, W.J. Niessen, K.L. Vincken, M.A. Viergever, W. William, C. Alan, D. Scott, Multiscale vessel enhancement filtering, in: *Medical Image Computing and Computer-Assisted Intervention MICCAI™98*, Springer, Berlin/Heidelberg, 1998, p. 130.
- [71] M.E. Martinez-Perez, A.D. Hughes, A.V. Stanton, S.A. Thom, A.A. Bharath, K.H. Parker, Retinal blood vessel segmentation by means of scale-space analysis and region growing, in: *Proceedings of the Second International Conference on Medical Image Computing and Computer-Assisted Intervention*, Springer-Verlag, London, UK, 1999, pp. 90–97.
- [72] M.E. Martinez-Perez, A.D. Hughes, S.A. Thom, A.A. Bharath, K.H. Parker, Segmentation of blood vessels from red-free and fluorescein retinal images, *Medical Image Analysis* 11 (2007) 47–61.
- [73] M.E.M. Perez, A.D. Hughes, S.A. Thorn, K.H. Parker, Improvement of a retinal blood vessel segmentation method using the Insight Segmentation and Registration Toolkit (ITK), in: *Engineering in Medicine and Biology Society, 2007. EMBS 2007. 29th Annual International Conference of the IEEE*, 2007, pp. 892–895.
- [74] O. Wink, W.J. Niessen, M.A. Viergever, Multiscale vessel tracking, *IEEE Transactions on Medical Imaging* 23 (2004) 130–133.
- [75] M. Sofka, C.V. Stewart, Retinal vessel centerline extraction using multiscale matched filters, confidence and edge measures, *IEEE Transactions on Medical Imaging* 25 (2006) 1531–1546.
- [76] A. Anzalone, F. Bizzarri, M. Parodi, M. Storage, A modular supervised algorithm for vessel segmentation in red-free retinal images, *Computers in Biology and Medicine* 38 (2008) 913–922.

- [77] D.J.J. Farnell, F.N. Hatfield, P. Knox, M. Reakes, S. Spencer, D. Parry, S.P. Harding, Enhancement of blood vessels in digital fundus photographs via the application of multiscale line operators, *Journal of the Franklin Institute* 345 (2008) 748–765.
- [78] M. Vlachos, E. Dermatas, Multi-scale retinal vessel segmentation using line tracking, *Computerized Medical Imaging and Graphics* 34 (2009) 213–227.
- [79] K.A. Vermeer, F.M. Vos, H.G. Lemij, A.M. Vossepoel, A model based method for retinal blood vessel detection, *Computers in Biology and Medicine* 34 (2004) 209–219.
- [80] V. Mahadevan, H. Narasimha-Iyer, B. Roysam, H.L. Tanenbaum, Robust model-based vasculature detection in noisy biomedical images, *IEEE Transactions on Information Technology in Biomedicine* 8 (2004) 360–376.
- [81] W. Li, A. Bhalerao, R. Wilson, Analysis of retinal vasculature using a multiresolution Hermite model, *IEEE Transactions on Medical Imaging* 26 (2007) 137–152.
- [82] B.S.Y. Lam, Y. Hong, A novel vessel segmentation algorithm for pathological retina images based on the divergence of vector fields, *IEEE Transactions on Medical Imaging* 27 (2008) 237–246.
- [83] B.S.Y. Lam, G. Yongsheng, A.W.C. Liew, General retinal vessel segmentation using regularization-based multiconcavity modeling, *IEEE Transactions on Medical Imaging* 29 (2010) 1369–1381.
- [84] H. Narasimha-Iyer, J.M. Beach, B. Khoobehi, B. Roysam, Automatic identification of retinal arteries and veins from dual-wavelength images using structural and functional features, *IEEE Transactions on Biomedical Engineering* 54 (2007) 1427–1435.
- [85] T. Zhu, Fourier cross-sectional profile for vessel detection on retinal images, *Computerized Medical Imaging and Graphics* 34 (2010) 203–212.
- [86] L. Espona, M.J. Carreira, M. Ortega, M.G. Penedo, A snake for retinal vessel segmentation, in: *Proceedings of the 3rd Iberian conference on Pattern Recognition and Image Analysis, Part II*, Springer-Verlag, Girona, Spain, 2007.
- [87] L. Espona, M.J. Carreira, M.G. Penedo, M. Ortega, Retinal vessel tree segmentation using a deformable contour model, in: *ICPR 2008. 19th International Conference on Pattern Recognition*, 2008, 2008, pp. 1–4.
- [88] B. Al-Diri, A. Hunter, D. Steel, An active contour model for segmenting and measuring retinal vessels, *IEEE Transactions on Medical Imaging* 28 (2009) 1488–1497.
- [89] K.W. Sum, P.Y.S. Cheung, Vessel extraction under non-uniform illumination: a level set approach, *IEEE Transactions on Biomedical Engineering* 55 (2008) 358–360.
- [90] Y. Zhang, W. Hsu, M. Lee, Detection of retinal blood vessels based on nonlinear projections, *Journal of Signal Processing Systems* 55 (2009) 103–112.
- [91] C. Alonso-Montes, D.L. Vilarino, M.G. Penedo, CNN-based automatic retinal vascular tree extraction, in: *9th International Workshop on Cellular Neural Networks and Their Applications*, 2005, pp. 61–64.
- [92] C. Alonso-Montes, D.L. Vilarino, P. Dudek, M.G. Penedo, Fast retinal vessel tree extraction: a pixel parallel approach, *International Journal of Circuit Theory and Applications* 36 (2008) 641–651.
- [93] M.A. Palomera-Perez, M.E. Martinez-Perez, H. Benitez-Perez, J.L. Ortega-Arjona, Parallel multiscale feature extraction and region growing: application in retinal blood vessel detection, *IEEE Transactions on Information Technology in Biomedicine* 14 (2010) 500–506.
- [94] S. Gregory, D. Trevor, I. Piotr, *Nearest-Neighbor Methods in Learning and Vision: Theory and Practice* (Neural Information Processing), MIT Press, 2006.
- [95] M.E. Martinez-Perez, A.D. Highes, A.V. Stanton, S.A. Thorn, N. Chapman, A.A. Bharath, K.H. Parker, Retinal vascular tree morphology: a semi-automatic quantification, *IEEE Transactions on Biomedical Engineering* 49 (2002) 912–917.
- [96] W.T. Freeman, E.H. Adelson, The design and use of steerable filters, *IEEE Transactions on Pattern Analysis and Machine Intelligence* 13 (1991) 891–906.
- [97] L. Thomas, M.K. Jason, *Image Processing Using Pulse-Coupled Neural Networks*, Springer-Verlag Inc., New York, 1998.
- [98] D. Marco, S. Thomas, *Ant Colony Optimization*, Bradford Company, 2004.
- [99] J. Serra, *Image Analysis and Mathematical Morphology*, Academic Press, Inc., Orlando, FL, USA, 1983.
- [100] A.J. Baddeley, I.S. Molchanov, A.J. Baddeley, I.S. Molchanov, Averaging of random sets based on their distance functions, *Journal of Mathematical Imaging and Vision* 8 (1995) 79–92.
- [101] H.S. Dietrich Stoyan, *Fractals Random Shapes and Point Fields: Methods of Geometrical Statistics*, John Wiley & Sons, New York, 1994.
- [102] G. Xiaohong, A. Bharath, A. Stanton, A. Hughes, N. Chapman, S. Thom, A method of vessel tracking for vessel diameter measurement on retinal images, in: *Proceedings. 2001 International Conference on Image Processing*, 2001, vol. 882, 2001, pp. 881–884.
- [103] S. Hong, B. Roysam, C.V. Stewart, J.N. Turner, H.L. Tanenbaum, Optimal scheduling of tracing computations for real-time vascular landmark extraction from retinal fundus images, *IEEE Transactions on Information Technology in Biomedicine* 5 (2001) 77–91.
- [104] W.A. Barrett, E.N. Mortensen, Interactive live-wire boundary extraction, *Medical Image Analysis* 1 (1997) 331–341.
- [105] L. Ibanez, W. Schroeder, L. Ng, J. Cates, *The ITK Software Guide*, Kitware, Inc., 2003, ISBN 1-930934-10-6, <http://www.itk.org/itkSoftwareGuide.pdf>.
- [106] P.J. Huber, A robust version of the probability ratio test, *Annals of Mathematical Statistics* 36 (1965) 1753–1758.
- [107] C. Field, B. Smith, Robust estimation – a weighted maximum-likelihood approach, *International Statistical Review* 62 (1994) 405–424.
- [108] E. Ronchetti, Robust model selection in regression, *Statistics & Probability Letters* 3 (1985) 21–23.
- [109] H. Narasimha-Iyer, V. Mahadevan, J.M. Beach, B. Roysam, Improved detection of the central reflex in retinal vessels using a generalized dual-gaussian model and robust hypothesis testing, *IEEE Transactions on Information Technology in Biomedicine* 12 (2008) 406–410.
- [110] P. Kovsi, Phase congruency detects corners and edges, in: *The Australian Pattern Recognition Society Conference: DICTA 2003*, 2003, pp. 309–318.
- [111] M. Kass, A. Witkin, D. Terzopoulos, Snakes: active contour models, *International Journal of Computer Vision* 1 (1988) 321–331.
- [112] B. Al-Diri, A. Hunter, A ribbon of twins for extracting vessel boundaries, in: *The 3rd European Medical and Biological Engineering Conference*, Prague, Czech Republic, 2005.
- [113] T.F. Chan, L.A. Vese, Active contours without edges, *IEEE Transactions on Image Processing* 10 (2001) 266–277.
- [114] C.S. Tong, Y. Zhang, N. Zheng, Variational image binarization and its multi-scale realizations, *Journal of Mathematical Imaging and Vision* 23 (2005) 185–198.
- [115] L.O. Chua, L. Yang, Cellular neural networks: theory, *IEEE Transactions on Circuits and Systems* 35 (1988) 1257–1272.
- [116] T. Roska, L.O. Chua, The CNN universal machine: an analogic array computer, *IEEE Transactions on Circuits and Systems II: Analog and Digital Signal Processing* 40 (1993) 163–173.

- [117] D.L. Vilarino, C. Rekeczky, Pixel-level snakes on the CNNUM: algorithm design, on-chip implementation and applications, *International Journal of Circuit Theory and Applications* 33 (2005) 17–51.
- [118] C. Rekeczky, MATCNN – Analogic Simulation Toolbox for Matlab, in *Analogic and Neural Computing Laboratory, Computer and Automation Institute*, 1997.
- [119] P. Dudek, S.J. Carey, General-purpose  $128 \times 128$  SIMD processor array with integrated image sensor, *Electronics Letters* 42 (2006) 678–679.
- [120] D.L. Vilarino, C. Rekeczky, Implementation of a pixel-level snake algorithm on a CNNUM-based chip set architecture, *IEEE Transactions on Circuits and Systems I: Regular Papers* 51 (2004) 885–891.
- [121] P. Renzo, R. Elisa, C. Daniele, C. Giovanni, Cellular neural networks with virtual template expansion for retinal vessel segmentation, *IEEE Transactions on Circuits and Systems II: Express Briefs* 54 (2007) 141–145.
- [122] G. Costantini, D. Casali, M. Todisco, A hardware-implementable system for retinal vessel segmentation, in: *Proceedings of the 14th WSEAS International Conference on Computers: Part of the 14th WSEAS CSCC Multiconference, vol. II, World Scientific and Engineering Academy and Society, WSEAS, Stevens Point, Wisconsin, USA, 2010*, pp. 568–573.
- [123] R. Zwigelaar, S.M. Astley, C.R.M. Boggis, C.J. Taylor, Linear structures in mammographic images: detection and classification, *IEEE Transactions on Medical Imaging* 23 (2004) 1077–1086.
- [124] G. Linan, A. Rodriguez-Vazquez, S. Espejo, R. Dominguez-Castro, ACE16K: a  $128 \times 128$  focal plane analog processor with digital I/O, in: *Proceedings of the 2002 7th IEEE International Workshop on Cellular Neural Networks and Their Applications, (CNNA 2002)*, 2002, pp. 132–139.
- [125] R. Rangayyan, X. Zhu, F. Ayres, A. Ells, Detection of the optic nerve head in fundus images of the retina with gabor filters and phase portrait analysis, *Journal of Digital Imaging* 23 (2010) 438–453.
- [126] M.Z.C. Azemin, D.K. Kumar, T.Y. Wong, R. Kawasaki, P. Mitchell, J.J. Wang, Robust methodology for fractal analysis of the retinal vasculature, *IEEE Transactions on Medical Imaging* 30 (2011) 243–250.
- [127] M. Ortega, N. Barreira, J. Novo, M.G. Penedo, A. Pose-Reino, F. Gómez-Ulla, Sirius: a web-based system for retinal image analysis, *International Journal of Medical Informatics* 79 (2010) 722–732.
- [128] C.V. Stewart, B. Roysam, RIVERS: Retinal Image Vessel Extraction and Registration System, <http://cgi-vision.cs.rpi.edu/cgi/RIVERS/index.php.in>.
- [129] C.L. Tsai, B. Madore, M.J. Leotta, M. Sofka, G. Yang, A. Majerovics, H.L. Tanenbaum, C.V. Stewart, B. Roysam, Automated retinal image analysis over the internet, *IEEE Transactions on Information Technology in Biomedicine* 12 (2008) 480–487.
- [130] A. Perez-Rovira, T. MacGillivray, E. Trucco, K.S. Chin, K. Zutis, C. Lupascu, D. Tegolo, A. Giachetti, P.J. Wilson, A. Doney, B. Dhillon, VAMPIRE: vessel assessment and measurement platform for images of the RETina, in: *Engineering in Medicine and Biology Society, EMBC, 2011 Annual International Conference of the IEEE*, 2011, pp. 3391–3394.
- [131] A. Mosher, B.E.K. Klein, R. Klein, M.D. Knudtson, N.J. Ferrier, Comparison of retinal vessel measurements in digital vs film images, *American Journal of Ophthalmology* 142 (2006) 875–878.
- [132] C.M. Wilson, K.D. Cocker, M.J. Moseley, C. Paterson, S.T. Clay, W.E. Schulenburg, M.D. Mills, A.L. Ells, K.H. Parker, G.E. Quinn, A.R. Fielder, J. Ng, Computerized analysis of retinal vessel width and tortuosity in premature infants, *Investigative Ophthalmology & Visual Science* 49 (2008) 3577–3585.
- [133] C.G. Owen, A.R. Rudnicka, R. Mullen, S.A. Barman, D. Monekosso, P.H. Whincup, J. Ng, C. Paterson, Measuring retinal vessel tortuosity in 10-year-old children: validation of the Computer-Assisted Image Analysis of the Retina (CAIAR) Program, *Investigative Ophthalmology & Visual Science* 50 (2009) 2004–2010.
- [134] OptoMap Image Library, <http://www.optos.com/en-us/Professionals/Image-library/>, Optos Plc.
- [135] A. Perez-Rovira, K. Zutis, J.P. Hubschman, E. Trucco, Improving vessel segmentation in ultra-wide field-of-view retinal fluorescein angiograms, in: *Engineering in Medicine and Biology Society, EMBC, 2011 Annual International Conference of the IEEE*, 2011, pp. 2614–2617.